A STUDY OF OFDM IN UNDERWATER WIRELESS OPTICAL AND ACOUSTIC COMMUNICATIONS

By

ZHUORAN QI

A thesis submitted to the

School of Graduate Studies

Rutgers, The State University of New Jersey

In partial fulfillment of the requirements

For the degree of

Master of Science

Graduate Program in Electrical and Computer Engineering

Written under the direction of

Dario Pompili

And approved by

_____

_____

_____

New Brunswick, New Jersey

October 2019

ABSTRACT OF THE THESIS

A Study of OFDM in Underwater Wireless Optical and Acoustic Communications

by ZHUORAN QI

Thesis Director:

Prof. Dario Pompili

With the development of marine applications in military and commercial fields, underwater communication techniques with high transmission data rate over long-range distances are in urgent demand. Two mainstream underwater wireless communications solutions are Underwater Acoustic Wireless Communications (UAWC) and Underwater Optical Wireless Communications (UOWC), which are based on acoustic and optical signals, respectively. In this thesis, a new physical-layer architecture is proposed for high-data-rate UOWC based on integrated hybrid Orthogonal Frequency Division Multiplexing (OFDM) and Pulse Position Modulation (PPM) with Time-Frequency (TF) spreading. Such architecture is engineered to increase the transmission range compared to basic OFDM systems thanks to the robustness of the nonlinear PPM modulation in wireless fading channels. Frame error rate performance and physical-layer throughput results are obtained using a custom-made physical-layer simulator built to emulate hardware performance. It is found that, with the proposed hybrid OFDM-PPM modulation scheme, the range is extended by over $10\ \mathrm{m}$ for a single transmitting light source, and by over $20\ \mathrm{m}$ for four transmitting light sources. Moreover, with the TF-spreading, the proposed architecture can improve the coverage by several folds compared to the case without spreading. Importantly, the Doppler effect is mitigated effectively by the combination of OFDM-PPM and TF-spreading, as

shown via thorough simulations. Besides, the implementation of UWAC has been studied with a testbed using universal software radio peripheral hardware device. The OFDM-based Single-Input and Single-Output and Multi-input and Multi-output are tested in a water tank and the pool at Sonny Werblin Recreation Center, Rutgers University. Data of experimental results are collected, and the performances of the testbed are evaluated. Moreover, the performances of using spatial multiplexing and spatial diversity techniques in a MIMO structure are analyzed.

ACKNOWLEDGEMENTS

I would first like to thank my thesis advisor Prof. Dario Pompili for his useful comments, remarks and engagement whenever I ran into a trouble spot or had a question about my research. Through the learning process of this master thesis, it is his consistent support and guidance that steered me in the right direction. Furthermore, I would like to thank Mr. Xueyuan Zhao and Mr. Mehdi Rahmati for sharing their valuable experience in research. Finally, I must express my very profound gratitude to my parents and my friends for providing me with unfailing support and continuous encouragement throughout my years of study.

TABLE OF CONTENTS

LIST OF TABLES

LIST OF FIGURES

CHAPTER 1
INTRODUCTION

Underwater communications are of vital importance to a wide variety of underwater robotics, such as Autonomous Underwater Vehicles (AUV) [1] and unmanned submarines [2]. The applications include natural resource detection, scientific ocean exploration, environmental monitoring, etc. In order to facilitate all these activities, high bandwidth and high information transfer rates are expected. However, compared with terrestrial and space links, underwater wireless links turn out to be more challenging. In atmospheric links, the Radio Frequency (RF) wave is always a good choice because of its high data rate, high bandwidth and its fast velocity. However, even though RF wave in underwater wireless communication can improve the data rate in short distances, it attenuates significantly with the increase of frequency especially in seawater, for radio wave cannot propagate well through good electrical conductors like saltwater [3]. Therefore, there are two categories of communication techniques proliferated in the underwater wireless communication research, based on either acoustic waves and wireless optical signals. The underwater acoustic wireless communication (UAWC) takes advantages in long coverage distance. However, UAWC is difficult with challenges in narrow available bandwidth (limited in a few kbps), high propagation latency, severe signal attenuation, multipath propagation delay, and fast fading caused by Doppler effect [4]. For underwater optical wireless communication (UOWC) system, the data rate can reach in Gbps scale for the distance of a few meters. Due to the water absorption and scatter effect caused by suspended particles, the UOWC also suffers a high attenuation but relatively lower compared with that of RF in long distances. Table 1.1 shows the comparison between the three underwater wireless communication techniques.

Table 1.1: Comparison between different underwater wireless communication techniques

Parameters	**RF**	**Acoustic**	**Optical**
Wave speed	$1500\ \mathrm{m/s}$	$2.26 \times 10^5\ \mathrm{km/s}$	$2.26 \times 10^5\ \mathrm{km/s}$
Propagation Latancy	Moderate	High	Low
Bandwidth	$\sim$ MHz	$\sim$ kHz	$10 - 150$ MHz
Transmission Data Rate	$\sim$ Mbps	$\sim$ kbps	$10 - 150$ Gbps
Distance	Up to $10\ \mathrm{m}$	Up to $1000\ \mathrm{km}$	$10 - 100\ \mathrm{m}$

1.1 Underwater Acoustic Wireless Communication

Due to the low attenuation of acoustic waves in water, the acoustic communications have been widely used in the underwater environment in recent years, with a coverage distance up to several km. However, the typical acoustic frequency band in use today is $10\ -\ 15\ \mathrm{kHz}$, so the transmission data rate is bottle-necked severely. Besides, the speed of acoustic waves underwater is as slow as $1500\ \mathrm{m/s}$, resulting in latency in the propagation. The challenges faced by the UAWC channel [5] can be summarized as follows:

- The attenuation increases rapidly with the increase of bandwidth, and the coverage distance largely depends on the bandwidth [6]. When the bandwidth is narrower than $1\ \mathrm{kHz}$, the distance can reach up to $100\ \mathrm{km}$; when the bandwidth is about $10\ \mathrm{kHz}$, the range is up to $10\ \mathrm{km}$; when the bandwidth is about $100\ \mathrm{kHz}$, the distance is shorter than $100\ \mathrm{m}$. On the one hand, during the propagation, the energy of acoustic signals will be absorbed underwater and transferred into heat. On the other hand, a spreading loss will increase with distances, leading to an increase of overall path loss.

- The noise in an underwater acoustic channel is composed of the ambient noise and the site-specific noise. The ambient noise usually presents in the background and can be approximated as Gaussian but not white noise. While the site-specific noise largely depends on particular places and contains non-Gaussian components.

- As a result of reflection and refraction in the water, the multipath delay occurs in

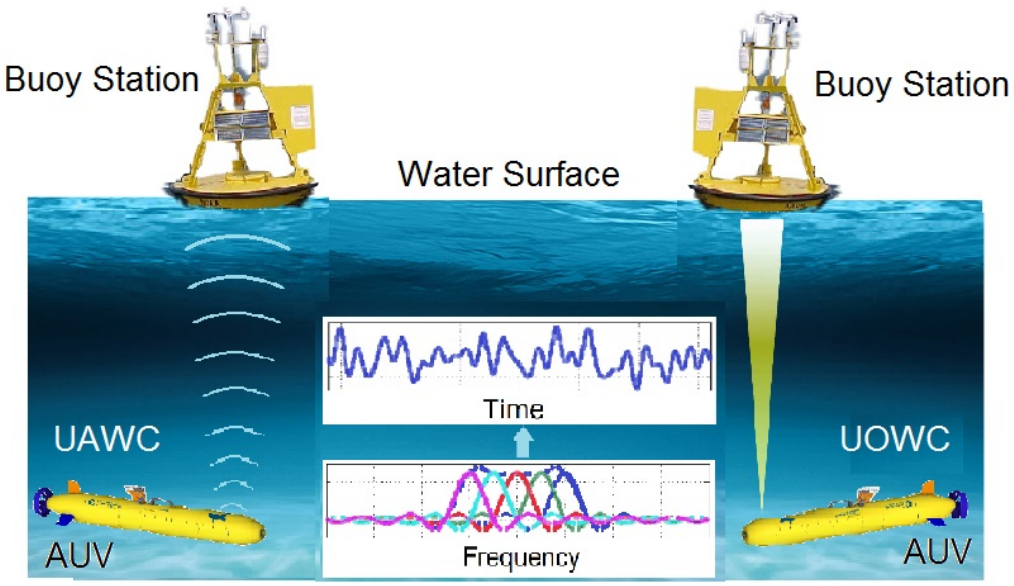

Figure 1.1: OFDM modulation applied in UAWC and UOWC, respectively

UAWC with a propagation latency around 10 ms [6]. Therefore, the frequency selective distortion exists in UAWC due to the delay spreading.

- The underwater acoustic channel is time-variant as a consequence of the constitutional changes in the propagation medium and the motion of transmitter and receiver. The latter is usually induced by the surface waves or the speed of AUV, which results in signal scattering effect and Doppler shift.

One of the most favorable communication schemes in UAWC is Orthogonal frequency-division multiplexing (OFDM), as shown in Figure 1.1. The OFDM takes advantages in low complexity at the receiver, resilience against frequency selective fading channel, and high bandwidth efficiency [7] by sending parallel data sequences on orthogonal subcarriers.

1.2 Underwater Optical Wireless Communication

In recent years, tremendous progress has been made in the field of the UOWC, bringing advantages in terms of a wide bandwidth—in the scale of hundreds of MHz—and a short transmission latency—in the scale of several ns. Nevertheless, the major bottleneck

of UOWC is the high attenuation of the optical signal in the water, due to absorption or scattering caused by particles and strong noise generated by the sunlight, which limits the coverage of the system [8, 9, 10]. Also, the Doppler shift caused by the moving AUV cannot be neglected due to the high carrier frequency at an optical frequency band.

In the field of UOWC, OFDM is also widely used. Another modulation scheme, called Pulse Position Modulation (PPM), is also studied in UOWC environment. Despite the progress in UOWC systems, problems remaining unsolved include:

- In OFDM frame structure, a large number of subcarriers are modulated independently, leading to a high Peak-to-Average Power Ratio (PAPR) and hence the OFDM modulation is sensitive to Inter-Carrier Interference (ICI) in Doppler channel.
- PPM has a low transmission data rate and a low spectrum efficiency.
- Channel estimation and tracking in OFDM systems consume pilot resources and reduce data transmission efficiency.
- Multi-Input Multi-Output (MIMO) scheme has not been considered for hybrid OFDM-PPM in UOWC.
- Doppler effects caused by AUV speeds are not investigated in OFDM-PPM system in UOWC.

1.3 Thesis Overview

In this thesis, the UAWC and UOWC are studied separately. For UOWC, we design a new physical-layer architecture that can achieve significant coverage extension of several folds compared with the ordinary OFDM system. We propose to employ a hybrid OFDM-PPM modulation scheme. A novel Time-Frequency (TF) spreading structure is also introduced to improve further the coverage distance based on OFDM. The results are generated based on MATLAB simulations. Contributions of this work are as follows.

- This is the first complete physical-layer optical architecture design with the hybrid OFDM-PPM modulation scheme and TF-spreading as critical features in UOWC, which aims at significantly improving the coverage distance as well as the frequency spectrum efficiency.

- For OFDM-PPM detection, the signal is conveyed by the non-linear modulation of pulse position in the time domain, and the receiver signal detector is to do peak detection to recover the pulse position. The equivalent channel with PPM is found to be additive Gaussian. Therefore the channel estimator and pilots are no longer needed in the proposed system.

- The physical-layer evaluation of the proposed new architecture is carried out under a realistic optical communication channel, including results of Frame Error Rates (FER) and physical-layer throughput at varying distances and different AUV moving speeds.

- The physical-layer simulation results indicate that the system achieves several folds' coverage extension compared with ordinary OFDM setups without spreading. The performance degradation caused by the Doppler effect is alleviated by the combination of hybrid OFDM-PPM modulation and TF-spreading.

Note that the light source in this study is assumed to be Light Emitting Diode (LED) sources. By adopting the LED source, the optical beam can cover all the photonic elements at the receiver. The laser source's positioning issue no longer exists if the LED source is assumed. In this design, we consider a $10\ \mathrm{GHz}$ sampling rate for the Digital-to-Analog Converter (DAC) at the transmitter and Analog-to-Digital Converter (ADC) at receiver for the PPM. Therefore the MIMO receiver is assumed as a small number (one or four) of photodetectors.

As for UAWC, the Universal Software Radio Peripherals (USRPs) and hydrophones are deployed to transmit and receive acoustic signals. Experiments and testing are done in

a water tank and the pool in Sonny Werblin Recreation Center, Rutgers University. The features of the work are as follows.

- The bit streams are modulated with OFDM modulation scheme with 100 kHz bandwidth in short distances. Channel estimation and Zero-Forcing (ZF) is utilized to decode the received data.

- For experiments in the tank, 1-by-1, 1-by-2, and 2-by-2 transmission schemes are tested. Different source codes (such as BPSK and QPSK) are tested separately. Also, Single-Input and Single-Output (SISO), Single-Input and Multiple-Output (SIMO), and MIMO transmission schemes are experimented. The performances of spatial diversity and spatial multiplexing are analyzed. The performances of Bit Error Rate (BER) and physical-layer throughput versus distances are presented.

- For experiments in the pool, the 1-by-1 transmission scheme is tested with BPSK modulation. The channel impulse responses are presented.

In chapter 2, we review the related works of UAWC and UOWC in recent years, including the MIMO-OFDM acoustic transmission schemes, acoustic MIMO space-time coding techniques, and time synchronization.

In chapter 3, we introduce the Line of Sight (LOS) UOWC channel model and design a new optical communication architecture, which can achieve significant coverage extension of several folds compared with the ordinary OFDM system. We propose to employ a hybrid OFDM-PPM scheme; a novel TF-spreading structure is also introduced to improve further the coverage distance based on OFDM modulation.

In chapter 4, we introduce the custom-made physical-layer simulator model and simulation scenarios. The parameters utilized in the simulation are detailedly explained. Different transmission schemes are tested with varying distances and different AUV speed. The results and findings, including FER and physical-layer throughput, are analyzed.

In chapter 5, we introduce the equipment we deploy for the UAWC testbed experiments, including the hydrophones and USRP. The experimental structure is described, and the parameters applied in experiments are presented. Four transmission schemes are tested, which are the 1-by-1 transmission, 1-by-2 spatial diversity, 2-by-2 Space-Time Block Coding (STBC) and 2-by-2 Verticle Bell Laboratories Layered Space Time (V-BLAST). The results and performances are presented, including BER and physical-layer throughput.

In chapter 6, we conclude from the experimental results and simulation results obtained in chapter 5 and chapter 4, and discuss the future work of UAWC testbed experiment and hybrid OFDM-PPM scheme improvement.

CHAPTER 2
RELATED WORK

In this chapter, we discuss the state of art of UAWC and UOWC, including the techniques of transmission schemes, channel estimation, time synchronization, channel modulation, as well as hardware experiments.

2.1 Underwater Acoustic Wireless Communication

In acoustic communications, our Cyber-Physical Systems Laboratory (CPS Lab) utilizes the hybrid automatic repeat request technique for reliable underwater acoustic MIMO communication [11]. A massive MIMO hydrophone array with carrier aggregation is proposed to significantly improve the coverage and data rate for UAWC systems [12]. The underwater acoustic carrier aggregation technique has been further investigated by simulations [13] and ocean experiments [14]. Adaptive underwater video transmission is proposed via software-defined MIMO acoustic modems [15], where USRP is utilized for testbed experiments.

There are existing proposals of other groups that adopt MIMO techniques in UAWC. Authors in [16] study the underwater acoustic MIMO and SIMO channel based on a remotely operated experimental platform. A series of offshore experiments are done based on the sea test base platform. The spectral efficiency gain brought by MIMO for UAWC is quantified. In work [17], a Carrier Interferometry (CI)/OFDM system in UAWC is designed and tested in a real underwater acoustic channel. The performances of the CI/OFDM and OFDM are compared based on PAPR and BER. It is found that the CI/OFDM can achieve better performance.

Regarding works on OFDM in UAWC, authors in [18] study the performance of Turbo Product Codes (TPC) and OFDM modulation in UAWC. The BELLHOP simulation model

has been used for getting the approximated actual response of the shallow underwater acoustic channel. The simulation results show that OFDM modulation based on TPC has excellent performance even in multipath and Doppler channel. The Alamouti space-frequency block coding is applied in UAWC-OFDM system in [19]. The authors propose an adaptive channel estimation method based on Doppler prediction and time smoothing. It is proven that the proposed scheme achieves an average mean square error gain of $2\ \mathrm{dB}$ compared with that of a single-transmitter scheme, and when the number of carriers is chosen optimally, the BER can be decreased by an order of magnitude. A Minimum-Mean-Square-Error (MMSE)-based OFDM transform-domain channel estimation is proposed for UAWC system in [20]. The system has been tested in a real underwater acoustic channel, with results showing that the transform-domain channel estimation can improve the performance of the UAWC-OFDM system. A high-speed UAWC system is designed based on OFDM in [21]. Experimental results show that it achieves data rate up to $9\ \mathrm{kbps}$ at $5\ \mathrm{km}$ and $2.8\ \mathrm{kbps}$ at $10\ \mathrm{km}$. Work [22] proposes a scalable OFDM design for UAWC, where one signal design can be easily scaled to fit into different transmission bandwidth with negligible changes on the receiver. The proposed scheme achieves a data rates from $12\ \mathrm{kbps}$ to $50\ \mathrm{kbps}$ with different bandwidth from $12\ \mathrm{kHz}$ to $50\ \mathrm{kHz}$.

The combination of MIMO and OFDM techniques have shown advantages in underwater acoustic communications. Authors in [23] present a MIMO-OFDM system design, where the receiver works on a block-by-block basis. The null subcarriers are used for Doppler compensation, and pilot subcarriers are used for channel estimation. The low-density parity-check is utilized for channel decoding. It achieves a communication data rate of $125.7\ \mathrm{kbps}$ over a bandwidth of $62.5\ \mathrm{kHz}$ with a spectral efficiency of $3.5\ \mathrm{bps/Hz}$. The Turbo-coded MIMO-OFDM system in UAWC environment is considered in [24]. The authors implement the Inverse Fast Fourier Transform (IFFT) block at the transmitter and Fast Fourier Transform (FFT) block at the receiver to realize multi-carrier modulation. Nonlinear detector based on the ZF algorithm is applied at the receiver. Authors in [25]

exploit the space time frequency diversity with MIMO-OFDM. It shows that when the spatial diversity is low, the coded modulation schemes emphasizing higher Hamming distance yield a lower error rate and when spatial diversity is high, coded modulation schemes emphasizing higher free Euclidean distance demonstrate a lower error rate.

For underwater acoustic channel estimation and equalization, the impulse noise and large-scale single frequency noise is studied for underwater acoustic OFDM in [26]. The authors estimate the impulse noise and large-scale single frequency noise separately. The simulation and experimental results show that the proposed method can effectively mitigate noise interference. In work [27], the joint carrier frequency offset and impulse noise is estimated with null subcarriers for OFDM in UAWC. Simulation results show that the joint estimation of carrier frequency offset and impulse noise has a better performance than the separated estimation. The channel equalization technique is studied for underwater acoustic channel [28], which proposes a new variable step-size least mean square (LMS) adaptive equalization algorithm. Authors in [29] compare different kinds of receiver window functions for suppressing narrowband interference (NBI) and finds that the raised cosine window can suppress the NBI and reduce the SNR. Authors in [30] also propose an underwater acoustic OFDM channel equalizer based on LMS adaptive algorithm.

As for time synchronization in UAWC, Pseudo Random (PN) Sequence is applied to an underwater acoustic orthogonal signal-division multiplex communication system [31]. Work [32] proposes a frame synchronization method for UAWC by involving transmitting signal based on hyperbolic frequency modulated signal as a preamble signal and using a correlator at the receiver to match the transmitted signal, which works with a robust correlation output of the Doppler effect as well as multi-path delay. Linear frequency modulation is adopted for time synchronization [33]. The scheme is implemented on the Field Programmable Gate Array (FPGA) and is implemented in the pool test, which shows the feasibility for the proposed scheme. Authors in [34] compare the performances of different time synchronization algorithms for UAWC-OFDM system, including maximum likeli-

hood (ML) algorithm based on Cyclic Prefix (CP), linear frequency modulation (LFM) and PN-sequence. Both computer simulation and testbed results show that ML based on CP is more sensitive to noise; PN-sequence leads to wrong judgments at receivers; LFM is suitable for UAWC-OFDM system.

2.2 Underwater Optical Wireless Communication

Regarding works on UOWC, a great number of experiments have been done, showing that the UOWC can achieve a high transmission data rate. Authors in [35] study the scintillations of red, green, and blue laser beams in various weak turbulent water channels. The threshold of turbulence in UOWC is learnt, and the BER is measured for the green laser, which shows that the UWOC link can still be retrievable in turbulent underwater environment if the turbulence is below a certain threshold. The development of high repetition rate multispectral LED optical systems for image and data transmission is discussed in [36], where the rate reaches $100\ \mathrm{kbps}$.

There are proposals discussing underwater optical OFDM applications. An LED-based UOWC system in shallow water is demonstrated in shallow water using OFDM and bit-loading algorithm [37], which achieves data rates of $158\ \mathrm{Mbps}$ in the daytime and $205\ \mathrm{Mbps}$ in the night-time over a coverage distance of $10\ \mathrm{m}$. Authors in [38] use Quadrature Amplitude Modulation (QAM)-OFDM modulation, which achieves a data rate of $1.118\ \mathrm{Gbps}$ and a spectral efficiency of $6.18\ \mathrm{bps/Hz}$. Experimental works [39] have shown that an OFDM-based laser communication system with 16-QAM modulation has achieved $8.8\ \mathrm{Gbps}$ transmission data rate over a transmission distance of $10\ \mathrm{m}$ based on light injection and optoelectronic feedback techniques. Work [40] proposes a 16-QAM-OFDM modulation scheme based on underwater blue laser communications, which has shown to achieve a transmission data rate of $9.6\ \mathrm{Gbps}$ over a distance of up to 8 meters. The two-stage injection-locked technique is also applied in this proposal and shows the feasibility of UOWC for long-range and high-speed links. A probabilistically shaped 256-QAM-OFDM transmission is

explored in [41]. The results show that it achieves 27.8% capacity improvement and a net data rate of around 12.64 Gbps compared with bit-power loading scheme in a distance of 35 m. Work [42] demonstrates an underwater optical wireless transmission of 405 ns and 968 Mbps optical Intensity Modulation/Direct Detection- OFDM signals with a distance of 2 m based on developed FPGA real-time transmitter. However, the ordinary OFDM exhibits large PAPR, which results in severe nonlinear distortion during the transmission.

For works discussing underwater optical MIMO applications, the BER performance under weak turbulence is analyzed for MIMO communications with Spatial Modulation (SM) [43]. Compared with convention MIMO using repetition code, the SM achieves improved spectral efficiency. Nevertheless, due to the differences between transmit-to-receive wireless links, the SM requires perfect channel knowledge for data detection, which introduces much complexity and high cost. MIMO capacity has been analyzed for the 2-by-2 optical system [44] and downlink underwater optical system [45]. MIMO has been proposed, and the error rate performance has been analyzed. Impulse response modeling of the optical MIMO channel has also been studied [46, 47]. The results show that the linear modulation suffers Inter-Symbol Interference (ISI) resulting from the temporal spread.

As for channel equalization, work [48] proposes an efficient analog post-equalizer to expand the bandwidth of the UOWC transmission system. A blue LED source is deployed with a bandwidth of 4 MHz, and a decoder is deployed with a bandwidth of 100 MHz. The proposed post-equalizer achieves a 745 Mbps transmission data rate with 64-QAM-OFDM modulation and a distance of 2 m. Authors in [49] present an adaptive approach to channel estimation based on Monte Carlo simulations for SISO-UOWC. On the other hand, UOWC channel model is further studied in recent years. A non-LOS scattering channel model is studied in work [50]. Mathematical modeling of UOWC is analyzed in work [51].

There are other transmission schemes researched for UOWC. On-Off Keying (OOK), Pulse Amplitude Modulation, PPM, and Pulse Width Modulation are studied for the blue-ray LED [52], where the distance is shorter than 5 m. Both simulation and real-world test-

ing results show that PPM is more power-efficient and able to maximize the Signal-to-Noise Ratio (SNR). Work [53] studies the communication performance of Flag Differential Pulse Position (F-DPPM), OOK, and Differential Pulse Position Modulation (DPPM), showing the advantages of F-DPPM in power spectral density and power efficiency. Work [54] introduces the Polarization Differential Pulse Position Modulation (P-DPPM) and compares against DPPM and OOK. The results show that it has high bandwidth efficiency and low FER. However, MIMO and OFDM modulation schemes are not considered, so the frequency spectrum efficiency and physical-layer throughput are limited. The hybrid OFDM-PPM technique applied for free-space-optical communication is investigated in [55]. This work shows that the OFDM-PPM is of higher power efficiency and lower PAPR compared with ordinary OFDM, but does not consider different cases of MIMO schemes and has not been proven for underwater communications.

CHAPTER 3
UNDERWATER OPTICAL WIRELESS COMMUNICATION PROPOSAL

To improve the communication coverage for UOWC, we propose a new architecture that enhances the robustness of the system by deploying the hybrid OFDM-PPM modulation. First, we spread the constellation signals in the TF-domain with orthogonal codes (e.g., Hadamard code). The OFDM modulation places the constellation signals in frequency in a conjugate-symmetric way, then converts the signals from frequency-domain to time-domain resulting in real-valued signals. Since the signals in the time domain are real-valued, the amplitude can directly modulate the pulse position by mapping the amplitude values into their corresponding quantized values. If each PPM frame has N_{PPM} time slots, there are N_{PPM} quantized values in total while different values correspond to different time delays.

To address the possible misalignment problem between the drifting transceivers caused by the waves, we map the PPM frames to spatial diversity transmission scheme, where duplicated signals are transmitted at each light source simultaneously. At the receiver, the smoothing filter is introduced to cancel the influence of the noise. With the work of smoothing filter, the interest signal of each PPM frame will be easily demodulated by simply analyzing the position of the maximum peak of each PPM frame. Besides, in flat fading channel, the received signal is composed of the same PPM signals with different multipath delay and additive noise, we only need to process it in the time domain without any channel estimator. Therefore, the complexity and cost are reduced. Moreover, due to TF-spreading, the Doppler effect caused by the mobile AUV is mitigated, and the SNR is improved at the receiver as well.

We now illustrate our proposed architecture in detail, including our novel contributions, i.e., the spatial diversity scheme based on PPM signals (Sect. 3.2), the hybrid OFDM-PPM

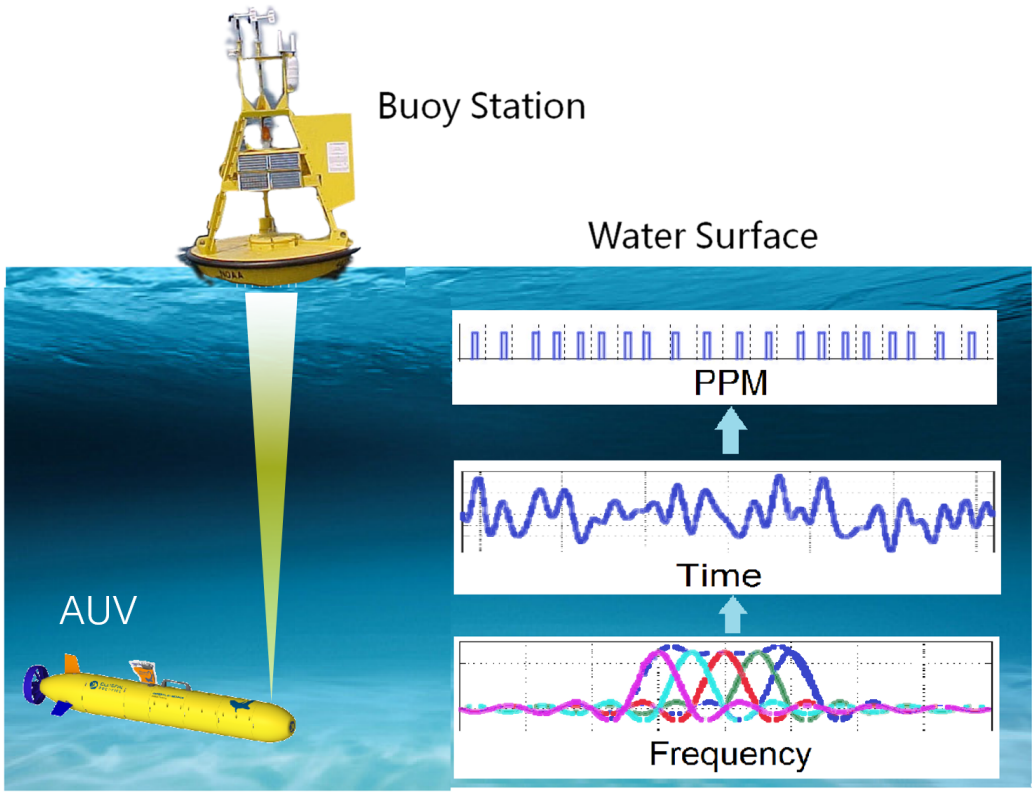

Figure 3.1: Transmitted hybrid OFDM-PPM signal processing.

modulator at the transmitter and demodulator at the receiver respectively (Sect. 3.3), and a TF-spreading at the transmitter (Sect. 3.4). Based on rigorous analyses, we derive the formula of the theoretical signal to noise ratio with the combination of the OFDM-PPM modulation scheme and TF-spreading.

3.1 Underwater Optical Channel

We discuss here the components of the underwater optical noise sources and model mathematically the power of the received optical signal. The noise in the underwater optical wireless communication system is composed of four main components [4]: 1) solar background noise; 2) shot noise; 3) dark current noise; 4) thermal noise [56].

1. The solar background noise arises from reflected and scattered solar background radiations during daytime observations. Assume N_{Solar} is the power of solar background

noise, in W,

$$N_{Solar} = (\eta_S S_a R_S)^2, \tag{3.1}$$

where η_S is the solar irradiance in the unit of $\mathrm{W/mm^2}$; S_a is the aperture area of photodetectors in the unit of $\mathrm{mm^2}$; R_S is the receiver sensitivity in the unit of $\mathrm{A/W}$.

2. The shot noise originates from the discrete nature of electric charge. Assume N_{Shot} is the power of the shot noise, in W,

$$N_{Shot} = 2qI_{in}B_W, \tag{3.2}$$

where q is the electronic charge of 1.6×10^{-19} C; I_{in} is the incident light current in the unit of A; B_W is the electronic bandwidth in the unit of Hz.

3. The dark current noise is from the random generation of electrons and holes within the depletion region of the device. Assume N_{Dark} is the power of the dark current noise, in W,

$$N_{Dark} = 2qI_{pd}B_W, \tag{3.3}$$

where I_{pd} is the photodiode parameter in the unit of A.

4. The thermal noise is generated by the thermal agitation of the charge carriers (usually the electrons) in the electrical and photonic devices. Assume N_{Ther} is the power of thermal noise, in W,

$$N_{Ther} = 4KTB_W/R_{Load}, \tag{3.4}$$

where K is the Boltzmann constant of 1.38×10^{-23} J/K; T is the temperature in the unit of K; R_{Load} is the load resistance in the unit of Ω.

Hence, the total noise power in the optical channel is assumed to be Additive White

Gaussian Noise (AWGN), which is expressed by summing these four components, i.e.,

$$N_{Total} = N_{Solar} + N_{Shot} + N_{Dark} + N_{Ther} \tag{3.5}$$

To simplify the transmission model while keeping realistic, we assume the transmission link to be a direct LOS from the transmitter to the receiver, and the environment is assumed to be the deep, dark and clear ocean. Considering the effect of scattering, dispersion and beam steering, we can express the power of the received optical signal by,

$$P_{R-LOS}(d) = P_{Trans} R_S \eta_T \eta_R L_p \frac{S_a \cos\theta}{\pi d^2 (1 - \cos\theta_0)} \tag{3.6}$$

where P_{Trans} is the transmit power at an AUV in the unit of W; η_T and η_R are the optical efficiency of the transmitter and receiver; θ is the transmitter inclination angle in the unit of degree; θ_0 is the LED beam divergence angle in the unit of degree; d is the distance of the range between transmitter and receiver in the unit of m; L_p is the propagation loss factor in the unit of m^{-1}, $L_p = \exp\{-c(\lambda)d\}$, where c is the beam extinction coefficient, which is a function of water type and wavelength λ. Hence, based on (3.5) and (3.6), the SNR of an underwater optical link at a distance d in the unit of m between a transmitter and a receiver is,

$$\begin{aligned} SNR(d) &= \frac{P_{R-LOS}(d)}{N_{Total}} \\ &= \frac{P_{Trans} R_S \eta_T \eta_R L_p \frac{S_a \cos\theta}{\pi d^2 (1-\cos\theta_0)}}{(\eta_S S_a R_S)^2 + 2q(I_{in} + I_{pd}) B_W + 4KTB_W / R_{Load}}. \end{aligned} \tag{3.7}$$

Note that there still might be solar background noise even in deep and dark water. The power of solar background noise is calculated by (3.1). The values of the parameters stated in above equations are chosen according to [57] and [58], as shown in Table 3.1. The water is assumed to be a deep dark clear ocean with a beam extinction coefficient of $c = 0.151$; the transmitting AUV is assumed to have a speed of 0.1 or 0.4 $\mathrm{m/s}$. The attenuation is

Table 3.1: UOWC Channel Model Parameters.

Parameters	**Value**
Underwater Environment	Deep, Dark Ocean
Solar Irradiance η_S	$0.81\ \mathrm{W/mm^2}$
Aperture Area of Photodetectors S_a	$0.01\ \mathrm{mm^2}$
Receiver Sensitivity R_S	$0.5\ \mathrm{A/W}$
Incident Light Current I_{in}	$25\ \mathrm{A}$
Electronic Bandwidth B_W	$100\ \mathrm{MHz}$
Photodiode Parameter I_{pd}	$1.226 \times 10^{-9}\ \mathrm{A}$
Temperature T	$290\ \mathrm{K}$
Load Resistance R_{Load}	$100\ \Omega$
Transmit Power at an AUV P_{Trans}	$50\ \mathrm{W}$
Optical Efficiency of the Transmitter η_T	0.9
Optical Efficiency of the Receiver η_R	0.9
Transmitter Inclination Angle θ	0^o
LED Beam Divergence Angle θ_0	68^o
Beam Extinction Coefficient in Clean Water c	0.151

firstly generated by (3.6); then, with Doppler shift and the effect of noise is added, which is composed of four major noise: sources solar background noise, shot noise, dark current noise and thermal noise. As for the optical noise model related parameters, the following values are chosen according to [57] and [58]. The solar irradiance η_S is assumed as $0.81\ \mathrm{W/mm^2}$; aperture area of each photodetectors S_a is $0.01\ \mathrm{mm^2}$; the receiver sensitivity R_S is $0.5\ \mathrm{A/W}$; the incident light current I_{in} is set as $25\ \mathrm{A}$; the electronic bandwidth B_W is $100\ \mathrm{MHz}$; the photodiode parameter I_{pd} is $1.226 \times 10^{-9}\ \mathrm{A}$; the temperature T is assumed to be $290\ \mathrm{K}$; the load resistance R_{Load} is $100\ \Omega$; the total transmit power P_{Trans} at an AUV is set as $50\ \mathrm{W}$; the optical efficiency of the transmitter η_T is 0.9 and the optical efficiency of the receiver η_R is 0.9; the transmitter inclination angle θ is assumed to be 0^o; the LED beam divergence angle θ_0 is assumed to be 68^o [58].

3.2 PPM-based Spatial Diversity

First, it should be noted that only one spatial stream is transmitted no matter for single or for multiple transmitting light sources. The spatial diversity strategy is applied. As a result, each light source transmits the same signal $s_{PPM}(t)$ in the current system model.

Then the received signal at the j-th photodetector $r_j(t)$ can be expressed as,

$$r_j(t) = \sum_{i=1}^{N_T} \sum_{m=1}^{N_{Path}} h_{ij}(t,m) s_{PPM}(t - \tau(m)) + n_j(t), \tag{3.8}$$

where $h_{ij}(t,m)$ denotes the channel impulse response between the i-th light source and j-th photodetector in the m-th path, $\tau(m)$ denotes the time delay of m-th path, $i = 1, 2, ..., N_T,\ j = 1, 2, ..., N_R,\ m = 1, 2, ..., N_{Path}$. N_T is the number of transmitting light sources. N_R is the number of photodetectors. N_{Path} is the number of paths. $n_j(t)$ represents the additive noise at the j-th photodetector.

With $h_j(t,m) = \sum_{i=1}^{N_T} h_{ij}(t,m)$, the received signal at the j-th photodetector can be

expressed by

$$r_j(t) = \sum_{m=1}^{N_{Path}} h_j(t,m) s_{PPM}(t - \tau(m)) + n_j(t). \tag{3.9}$$

Assume that the synchronization is ideal, we can process the received signals by adding them together,

$$r(t) = \sum_{j=1}^{N_R} r_j(t) = \sum_{m=1}^{N_{Path}} h(t,m) s_{PPM}(t - \tau(m)) + n(t), \tag{3.10}$$

where $h(t,m) = \sum_{j=1}^{N_R} h_j(t,m)$, $n(t) = \sum_{j=1}^{N_R} n_j(t)$.

Smoothing Filter: At the receiver, we introduce the moving average filter to smooth the data. The basic idea of the moving average filter is to replace each data points with the average of the N_{sps} neighboring data points. Note that N_{sps} is an odd number and is called a span of the filter. Assume $N_{sps} = 2k_s + 1$; then there are k_s neighboring data points on either side of the data point to be smoothed. When smoothing the p-th data point of the received data sequence,

$$r_{sm}(p) = \frac{1}{2k_s + 1} \sum_{k=-k_s}^{k_s} r(p + k). \tag{3.11}$$

3.3 Hybrid OFDM-PPM

In the wireless communication system, the OFDM has been widely used due to its robustness against the frequency selective fading channel; the spectrum efficiency is improved significantly by allowing overlapping as well. Also, the OFDM eliminates ISI through the use of a CP. However, the OFDM is more sensitive to the frequency offset due to the Doppler effect. As a result, ICI is introduced. Even though in UOWC where the transmission speed is very high (as high as 2.26×10^5 km/s) and the ICI are less severe compared with those in acoustic communication, the negative influence of ICI still exists.

It has been proven in related works [53, 54] that the PPM is quite useful in UOWC. In

PPM modulation, data are transmitted in the form of short pulses with the same width and amplitude, but the position of the pulses is in proportion to the amplitude of the message signal in the time domain. Therefore, all of the interest information is concentrated on the position of the peak per period. Moreover, the PPM modulation is nonlinear and can be implemented non-coherently. As for the linear signal with coherent detection, where the noise works on the transmitted symbols directly by introducing the phase offset, the accuracy of Phase-Shift Keying (PSK) demodulation can be influenced dramatically. In contrast, the PPM modulation doesn't need to track the carrier phase information. Instead, what we only care about is the peak position of the signal in each period, so that the high cost of phase detection can be discarded. Therefore, the phase offset caused by noise hardly has an impact on the PPM signal transmission.

Figure 3.1 depicts the hybrid OFDM-PPM modulation. First, we generate the OFDM signal in the frequency domain, after which we transfer the signal to time-domain. Then we modulate the signal with N_{PPM}-array PPM. Assume the OFDM signal at time t is $a(t) \in [-A, A]$, $(nT_d \leq t < (n+1)T_d,\ n = 0, 1, ...)$, the hybrid OFDM-PPM signal at time t is $s_{PPM}(t)$ [55],

$$s_{PPM}(t) = N_{PPM} \sum_{k=0}^{N_{PPM}} \mathrm{rect}(t - \frac{a_k(t)T_d}{N_{PPM}}), \tag{3.12}$$

where N_{PPM} is the number of time slots in each PPM frame, T_d is the frame duration of the OFDM-PPM scheme,

$$a_k(t) = \begin{cases} k, & \frac{2k}{N_{PPM}} - 1 \leq \frac{a(nT_d)}{A} < \frac{2(k+1)}{N_{PPM}} - 1, \\ & k = 0, 1, ..., N_{PPM} - 1 \\ 0, & otherwise \end{cases} \tag{3.13}$$

$$\mathrm{rect(t)} = \begin{cases} 1, & 0 \leq t < \frac{T_d}{N_{PPM}} \\ 0, & otherwise \end{cases} \tag{3.14}$$

At the receiver in reference to (3.10), the signal can be expressed by

$$r(t) = \begin{cases} N_{PPM} \sum_{m=1}^{N_{Path}} h(t - \tau(m), m) + n(t), & for\ a\ pulse\ time\ slot \\ n(t), & otherwise \end{cases} \tag{3.15}$$

where $h(t)$ and $n(t)$ are the channel impulse response and additive noise at time t. Since the detection algorithm at the receiver is to find the peak by time-domain filtering and peak detection, it is obvious that the SNR at the receiver is improved by N_{PPM} times.

To mitigate the multipath effect and to introduce a period for robust timing in a practical OFDM system; the CP is designed for hybrid OFDM-PPM. To optimize the CP length, we need to estimate the multipath effect in the optical channel. Note that the PPM is a non-linear modulation that will affect the multipath profile. Since the OFDM signal amplitude is determined by the pulse position in the time domain, the multipath and additive noise in the channel will affect the pulse position detection. This effect will introduce noise and another equivalent channel after PPM. There will be another channel profile that has different parameters other than the time-domain multipath channel. Therefore, it is necessary to evaluate what is the equivalent channel after the PPM modulation. A simple characterization can be done by generating known pilot OFDM symbols to PPM then to the multipath channel with noise, then do PPM demodulation and OFDM FFT. Then the frequency-domain channel responses can be estimated. This operation is performed for more than one thousand pilot OFDM symbols, and the resulting frequency-domain channel responses are averaged to obtain the frequency-domain channel estimate. The IFFT is performed to find the equivalent multipath channel response with PPM in the time domain.

3.4 Time-Frequency Spreading

The motivation to introduce the TF-spreading is that the SNR can be significantly improved and the Doppler effect can be effectively defended by spreading in the TF-domain [59]. Besides, the TF-spreading can be considered as a way to mitigate the ICI,

especially when the AUV speed is high.

Note that, multiplexing multiple users' signals will reduce the SNR. Given the transmit power constraint, if multiple users' signals are multiplexed in the spread code domain, the per-user power will have to be reduced by the factor of the number of code-domain multiplexed users. Reduced transmit power will subsequently cause reduced SNR at the receiver, therefore decreasing the throughput. So in the TF-spreading, only one user's signal is spread at the transmitter. We now provide the SNR analysis for the TF-spreading scheme [60].

Let us assume that the initial data bit sequence is converted from a serial to a parallel form, after which it is spread in the frequency domain with code $\mathbf{v}_i$ for the i-th parallel data stream, and spread in the time domain with code $\mathbf{u}$. Note that there is only one user in the system, meaning that different data streams will not be added together on the same OFDM subcarrier.

Let us now assume that the number of parallel data streams is N_c; the initial data is spread in the time domain with length L_T and is spread in the frequency domain with length L_F. Assuming $\mathbf{x}_i$ is the i-th parallel data stream after serial-to-parallel conversion, firstly it is spread in the frequency domain with code $\mathbf{v}_i$,

$$\mathbf{b}_i = \mathbf{v}_i \mathbf{x}_i = [v_{i,1}, v_{i,2}, ..., v_{i,L_F}]^T \mathbf{x}_i = [b_{i,1}, b_{i,2}, ..., b_{i,L_F}]^T. \tag{3.16}$$

Then each symbol in $\mathbf{b}_i$ is spread in the time domain with code $\mathbf{u}$. Thus, we get the following transmitted signal for each subcarrier,

$$\mathbf{s}_i = \mathbf{u}\mathbf{b}_i = [u_1, u_2, ..., u_{L_T}]^T \mathbf{b}_i, \tag{3.17}$$

where $\mathbf{v}$ and $\mathbf{u}$ are orthogonal codes, such as Hadamard Code.

The signals after TF-despreading are,

$$\widetilde{\mathbf{x}}_i = \frac{\mathbf{v}_i^H}{||\mathbf{v}_i||^2}\widetilde{\mathbf{b}}_i = \frac{\mathbf{v}_i^H}{||\mathbf{v}_i||^2}\frac{\mathbf{u}^H}{||\mathbf{u}||^2}\widetilde{\mathbf{s}}_i. \tag{3.18}$$

Therefore, thanks to this TF-spreading technique, we can improve the SNR at the receiver at the distance d, i.e.,

$$\gamma_{TFS}(d) = \frac{||\mathbf{u}||^4}{\mathbf{u}\mathbf{u}^H}\frac{||\mathbf{v}||^4}{\mathbf{v}\mathbf{v}^H}SNR(d) = L_T L_F SNR(d). \tag{3.19}$$

As stated in (3.19), the SNR after TF-despreading at the receiver is increased by $L_T L_F$ times w.r.t. the SNR of the combiner output without TF-spreading.

In this chapter, we analyze the model of underwater optical LOS channel. The components of Noise sources are explained, and the signal power attenuation is discussed. Our new architecture utilizes the techniques of MIMO based on the integrated hybrid OFDM-PPM transmission scheme and TF-spreading. In the following chapter 4, we present the simulation results of our proposed architecture with the FER and physical-layer throughput performances.

CHAPTER 4
PERFORMANCE EVALUATIONS OF UOWC PROPOSAL

As illustrated in chapter. 3, the hybrid OFDM-PPM and TF-spreading will improve the SNR significantly. In this chapter, we go further on the physical-layer simulator structure of our research by introducing in detail its parameters. Then, the simulation results of FER and physical-layer throughput will be plotted. The structure of our physical-layer simulator and the parameter settings of our simulator will be described. Note that Monte Carlo simulations are used and the results of the computer simulations with 95% confidence intervals are provided to ensure statistical relevance of the simulation results. Specifically, in Sect. 4.1, we describe the structure of our physical-layer simulator; in Sect. 4.2, we describe the parameter settings of our simulator; and in Sect. 4.3 we depict the results of the computer simulations with 95% confidence interval and provide a thorough analysis.

4.1 Custom-made Physical-layer Simulator

Before designing the proposed OFDM-PPM system structure, the wireless channel with PPM needs to be probed to characterize this channel. After channel probing, it is found that the channel only has an additive noise term added to the signal. Therefore, there is no need to design the channel estimator, pilots or the equalizer, since the constellation symbols are only affected by additive noise and the demodulator can recover the signal without performing equalization.

The structure of our custom-made physical-layer simulator is shown in Figure 4.1. At the transmitter, we first apply the channel coding (e.g., Turbo code), then adopt the interleaving technique to place the error bits sparsely in the data sequence. After base-band modulation, a Serial-to-Parallel (S/P) conversion is adopted. Then, TF-spreading is designed with orthogonal codes to spread in both time and frequency domains. Regarding

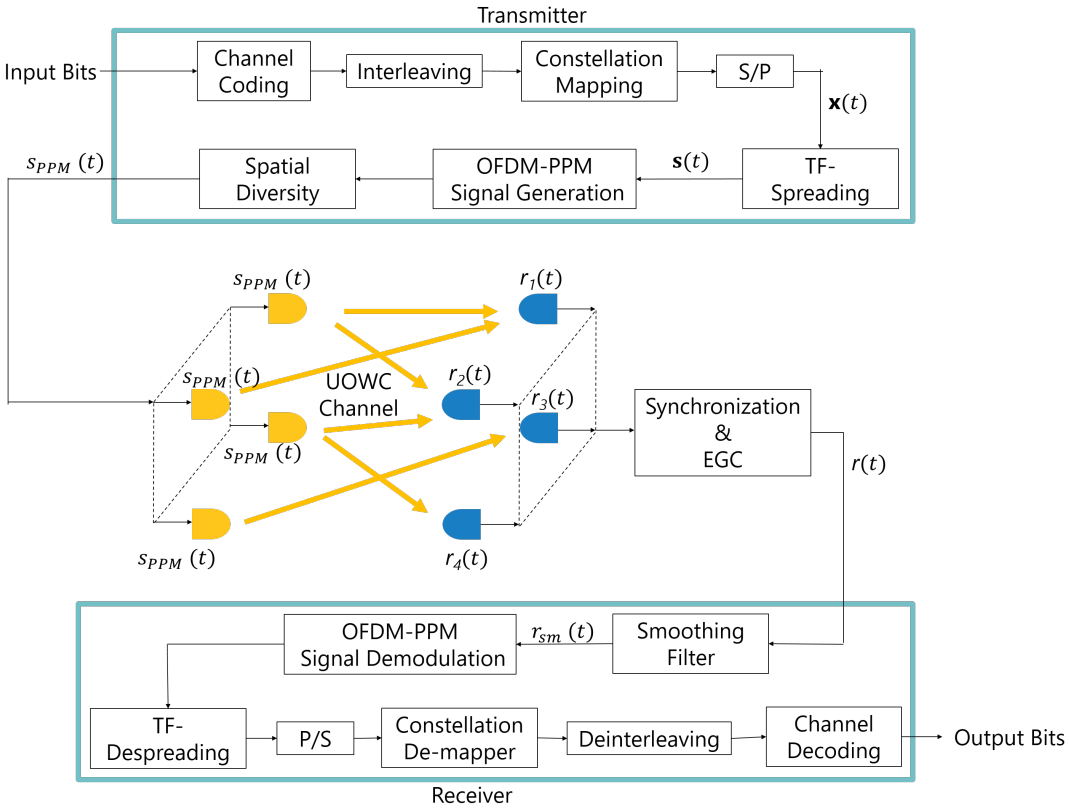

Figure 4.1: Structure of our simulator, including both transmitter and receiver side.

OFDM-PPM signal generation, we first generate OFDM frequency-domain symbols by placing the constellation symbols in a conjugate-symmetric way around the zero frequency, and then transform it into the time domain with IFFT. The conjugate-symmetric way ensures all real-valued time-domain signal. Then the time-domain signal is modulated with PPM and sent through multiple light sources. The signal is transmitted to multiple transmitting light sources with equal-gain transmitter diversity.

At the receiver, the time synchronization is done prior to receiver Equal-Gain Combining (EGC), and OFDM-PPM demodulation is subsequently performed. Since the equivalent channel with PPM only has additive noise effect, the receiver design is simplified, and no channel estimator or equalizer is needed. Then TF-despreading is applied to decode the signal to improve the receiver sensitivity and enhance the SNR at the receiver. The de-interleaving and channel decoding are then performed. The OFDM system design parameters in Table 4.1 are also adopted in the OFDM-PPM system.

4.2 Simulator Parameters Design

For the optical system, the optical beam is directional and does not have the effect of the ocean surface or bottom reflection. Nevertheless, there is still a scattering effect causing a minimal multipath delay. As shown in [6], for a UOWC system over a distance less than $100\ \mathrm{m}$, the transmission delay caused by the scattering effect will be equal or less than $\tau_{max} = 10\ \mathrm{ns}$. Considering the bandwidth of $100\ \mathrm{MHz}$ [6], we find that the introduced ISI will only affect one sample. Therefore, the number of paths is assumed to be 2, and the power delay varies with the distance between the AUV and buoy. The linear modulation of the OFDM optical signal can be realized by tuning of the LED beam photonic density. In existing optical systems adopting OOK modulation, very-high-speed ADC up to $10\ \mathrm{Gbps}$ can be designed. Therefore, we propose to apply the $10\ \mathrm{Gbps}$ for the PPM modulation. Due to the high cost of GHz-sampling-rate ADC, the number of photodetectors is limited at the receiver.

Table 4.1: UOWC Simulator Parameters.

Parameters	**Value**
Maximum Multipath Delay τ_{max}	10 ns
Number of Paths N_{Path}	2
AUV Speed	0.1 m/s or 0.4 m/s
Carrier Frequency f_c	4.75×10^5 GHz
Underwater Optical Speed v_c	2.26×10^5 km/s
Number of Photodetectors N_R	1 or 4
Number of Light Sources at AUV N_T	1 or 4
Baseband Modulation	QPSK
OFDM FFT-size K_{FFT}	64
Length of CP T_{CP}	20 ns
Channel Coding Rate R_{chc}	$1/3$
Time Period of OFDM Symbol T_{OFDM}	340 ns
Length of Time-Domain Spreading L_T	1 or 8
Length of Frequency-Domain Spreading L_F	1, 8 or 32
Number of PPM Time Slots N_{PPM}	100
Sampling Rate of ADC	10 GHz
Confidence Level	95%
Smoothing Filter Span N_{sps}	5

The channel model is established based on [4]. Parameters for the simulator are in Table 4.1. At the transmitter, we employ a red light LED with a carrier frequency of $f_c = 4.75 \times 10^5$ GHz and an underwater optical speed of $v_c = 2.26 \times 10^5$ km/s. On the number of photodetectors N_R, we assume it as 1 or 4. This scale is feasible from both an engineering and cost point of view. The channel coding rate is $R_{chc} = 1/3$. The length of time-domain spreading L_T is chosen to be 1 or 8, while the length of frequency-domain spreading L_F is chosen to be 1, 8, or 32. The number of time slots in the PPM frame N_{PPM} is chosen to be 100 so that the accuracy of PPM demodulation can be preserved. Note that the maximum tolerable clock drift is 0.4 ns.

The OFDM parameters are chosen according to the underwater multipath delay profile, as stated above. The multipath has a maximum delay of τ_{max}. The length of CP T_{CP} is related to the length of the OFDM symbol T_{OFDM} as $T_{OFDM} = \alpha T_{CP}$, where α is a constant. It is expected that the length of the OFDM symbol should be longer than the length of the CP. The OFDM system parameters are chosen according to the multipath power delay profile in underwater communication. Since the maximum multipath delay is 10 ns, we choose the CP length to be 20 ns to mitigate the ISI effect; the OFDM FFT size is chosen to be 64 with FFT duration of 640 ns. With the OFDM system bandwidth to be 100 MHz, overall the OFDM symbol length to be 660 ns, and the subcarrier spacing to be 1.56 MHz. FFT size and a CP length are fixed; this is because practical systems generally adopt fixed FFT size and a CP length.

4.3 Results and Findings

The major findings of the following simulation results include the coverage extension measured by FER. In Figures 4.2 to 4.13, which are based on the OFDM-PPM and ordinary OFDM modulation scheme, it is found that the coverage extension is improved by several folds, comparing the basic setup with the proposed architecture. Since the PPM converts the fading channel to additive Gaussian channel, there will be an equivalent SNR gain value

of the PPM, which contributes to the coverage improvement. Moreover, compared with the systems without TF-spreading, the systems with TF-spreading improve the coverage distance significantly due to the SNR gain of TF-spreading. For example, for $0.1\ \mathrm{m/s}$ AUV speed and 1-by-1 system, by the results of zero FER, the distance is increased from $6\ \mathrm{m}$ for ordinary OFDM without spreading, to $34\ \mathrm{m}$ for PPM-OFDM with TF-spreading. For $0.4\ \mathrm{m/s}$ AUV speed and 1-by-1 system, the distance is increased from $0\ \mathrm{m}$ for ordinary OFDM without spreading, to $32\ \mathrm{m}$ for OFDM-PPM with TF-spreading. For the 4-by-4 system, results also indicate several folds' coverage extension. Under $0.1\ \mathrm{m/s}$ AUV speed, the coverage is improved from $17\ \mathrm{m}$ for ordinary OFDM without spreading, to $49\ \mathrm{m}$ for OFDM-PPM with TF-spreading. Under $0.4\ \mathrm{m/s}$ AUV speed, the coverage is improved from $11\ \mathrm{m}$ for ordinary OFDM without spreading, to $48\ \mathrm{m}$ for OFDM-PPM with TF-spreading. These coverage extensions are determined by the FER results.

A frame is defined by consecutive 160 OFDM symbols, and the frame error occurs if a single bit in a frame is in error. There is another physical-layer performance metric evaluated, namely physical-layer throughput. The physical-layer throughput is calculated by,

$$Throughput = \frac{2^M K_{FFT} R_{chc}}{2 L_T L_F T_{OFDM}} (1 - FER), \tag{4.1}$$

where K_{FFT} is the FFT-size of OFDM; M the order of baseband modulation ($M = 2$ for QPSK); R_{chc} is the channel coding rate; FER is the frame error rate; T_{OFDM} is the period of one OFDM symbol. Comparing (3.19) with (4.1), we can find that, even though the SNR is improved by TF-spreading, the throughput is decreased, which shows an inherent engineering trade-off that needs to be navigated based on the applicsation.

Figures 4.2 to 4.13 depict the performance of SISO and MIMO systems, where the FER results indicate the coverage gain and a linear-scale is used to help emphasize the coverage distance. Figures 4.15 to 4.20 depicts the physical-layer throughput of different transmission schemes. The SISO system is defined as one light source and one photodetector, and the MIMO system is defined as one or four light sources and four photodetectors. The eval-

uations are done with QPSK modulation and AUV speeds of 0.1 and $0.4\ \mathrm{m/s}$. Note that, the physical-layer simulator is built to emulate practical hardware system implementation. The physical-layer simulation results can validate the effectiveness of our proposal and predict the performance in the real hardware system. We can find that the coverage distance gain of systems with four transmitting sources is twice as high as the gain of systems with only one transmitting source, as the multiple transmitting sources enhance the robustness of the system and solve the misalignment issues.

Figure 4.14 depicts the FER performances of systems without TF-spreading with an AUV speed of $0.1\ \mathrm{m/s}$. For 1-by-1 system, the coverage distance gain is about $15\ \mathrm{m}$ with OFDM-PPM, which almost triples the coverage distance with ordinary OFDM. For the 1-by-4 system, the coverage distance gain is about $10\ \mathrm{m}$ with OFDM-PPM. For the 4-by-4 system, the coverage distance gain is about $20\ \mathrm{m}$ with OFDM-PPM, which almost doubles the coverage distance with ordinary OFDM. Here we find that the coverage distance gain of systems with four transmitting sources is twice as high as the gain of systems with only one transmitting source. The reason is that the multiple transmitting sources enhance the robustness of the system.

To explore how Doppler effect influences the performance of our system, Figures 4.8 to 4.13 depicts the FER of OFDM-PPM and ordinary OFDM modulation systems with $0.4\ \mathrm{m/s}$ AUV speed respectively. Observing Figure 4.9, we find that the SISO system with ordinary OFDM without spreading doesn't work even at a distance as short as $1\ \mathrm{m}$, and the coverage of the other MIMO systems without spreading shrinks almost one half, which is attributed to the high Doppler effect caused by the high AUV speed. In Figure 4.12, we can see that there is a double coverage gain between 4-by-4 system without spreading and system with $L_F = 32,\ L_T = 8$, but this two scheme only has one half coverage gain when AUV speed is $0.1\ \mathrm{m/s}$. It shows that spreading in the TF-domain can mitigate the Doppler shift effectively. Moreover, comparing the FER performance of OFDM-PPM system with $0.1\ \mathrm{m/s}$ AUV speed and $0.4\ \mathrm{m/s}$ AUV speed, we find that the coverage distances only

shrink slightly when AUV speed is higher. However, for an ordinary OFDM system with higher AUV speed, the coverage distances shrink dramatically.

Figures 4.15 to 4.20 depicts the throughput performances of systems with OFDM-PPM and ordinary OFDM modulation. Note that there are intersection points on curves of physical-layer throughput, which are what we utilize to balance the number of photodetectors and the length of TF-Spreading versus distance. For $0.1\ \mathrm{m/s}$ AUV speed and 1-by-1 system with PPM-OFDM (Figure 4.15), the coverage distance is improved to $19\ \mathrm{m}$ with a throughput of $100\ \mathrm{Mbps}$ by OFDM-PPM without spreading, to $30\ \mathrm{m}$ with a throughput of $4\ \mathrm{Mbps}$ by frequency spreading, and to $34\ \mathrm{m}$ with a throughput of $500\ \mathrm{kbps}$ by TF-spreading. For $0.1\ \mathrm{m/s}$ AUV speed and 4-by-4 system with OFDM-PPM (Figure 4.19), the coverage distance is improved to $40\ \mathrm{m}$ with a throughput of $100\ \mathrm{Mbps}$ by OFDM-PPM without spreading, to $47\ \mathrm{m}$ with a throughput of $4\ \mathrm{Mbps}$ by frequency spreading, and to $49\ \mathrm{m}$ with a throughput of $500\ \mathrm{kbps}$ by TF-spreading. Comparing the throughput and coverage distance of OFDM-PPM and ordinary OFDM modulation, we can find that the maximum throughput for each setup with OFDM-PPM is the same as that with ordinary OFDM. Nevertheless, the OFDM-PPM improves the coverage distance significantly without sacrificing the physical-layer throughput. In addition, the physical-layer throughput curves can be applied to potential system adaptation on spreading parameters. Given a transmitter-receiver distance, the highest physical-layer throughput is determined from the curve data, and the adaptation of the spreading parameters is achieved.

In this chapter, we evaluate the performances of hybrid OFDM-PPM transmission scheme and TF-spreading. The proposed architecture is simulated with SISO, SIMO, and MIMO, respectively. Both FER and physical-layer throughput is analyzed. We find that the hybrid OFDM-PPM can improve the coverage distance by several folds, while TF-spreading improves the transmission range with a trade-off of physical-layer throughput. Although our proposed UOWC architecture realizes a high transmission data rate, the coverage distance is still limited, while UAWC is a good choice for long-distance transmission.

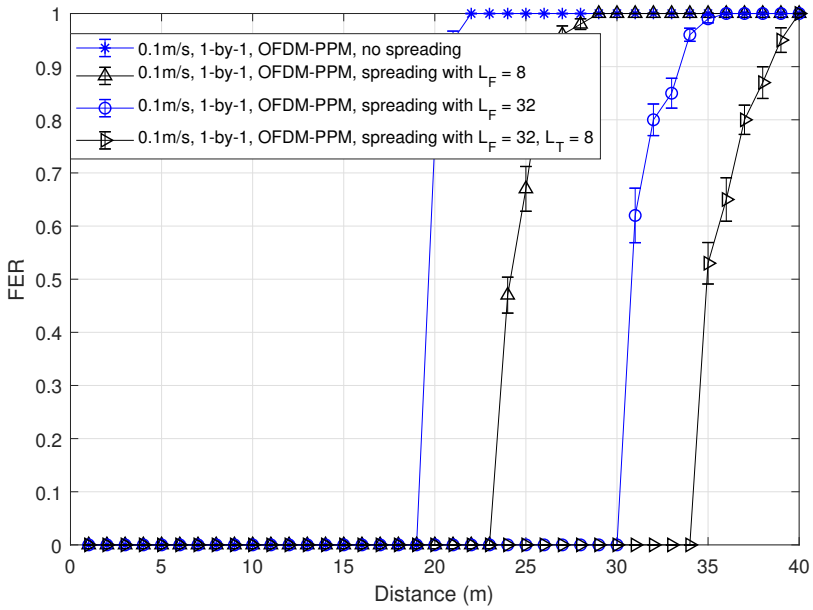

Figure 4.2: FER of 1-by-1 system with OFDM-PPM modulation when the AUV speed is $0.1\ \mathrm{m/s}$

To study the properties of UAWC, a series of UAWC-OFDM experiments are done in the chapter 5.

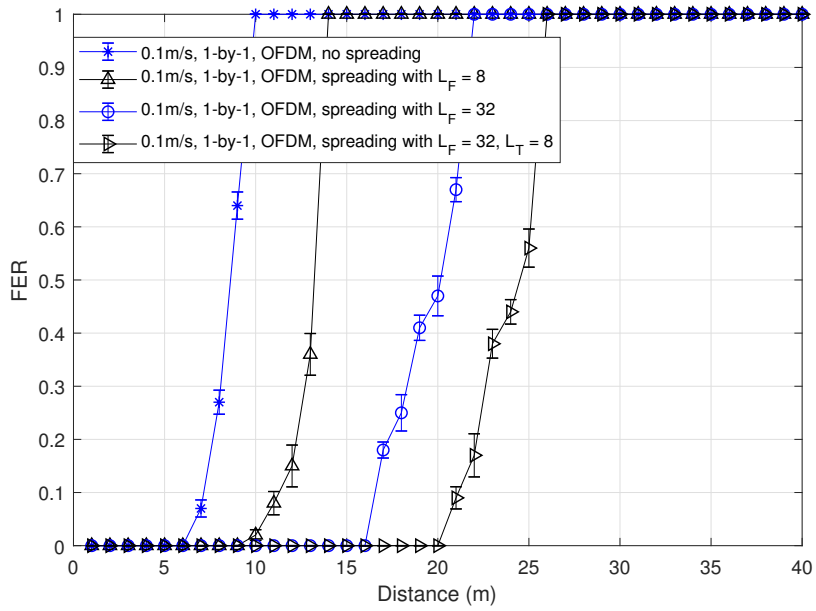

Figure 4.3: FER of 1-by-1 system with OFDM modulation when the AUV speed is $0.1\ \mathrm{m/s}$

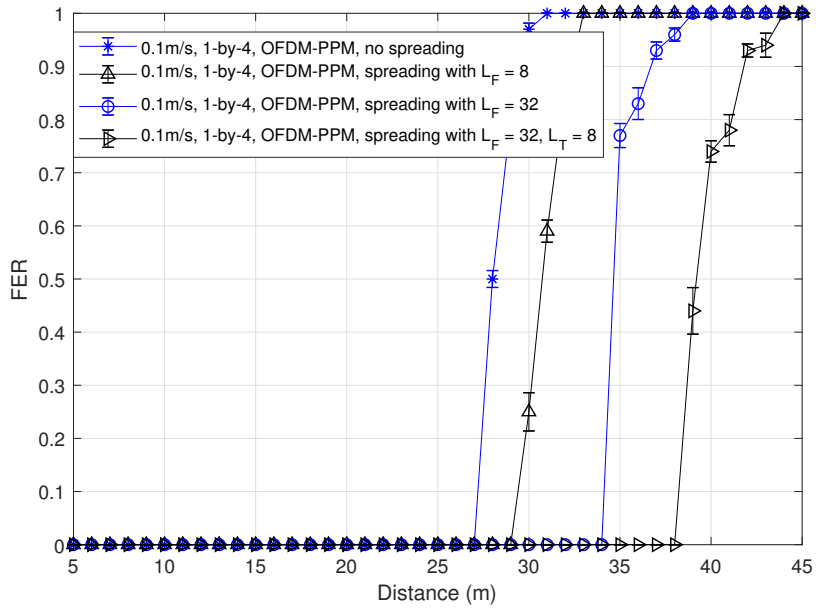

Figure 4.4: FER of 1-by-4 system with OFDM-PPM modulation when the AUV speed is $0.1\ \mathrm{m/s}$

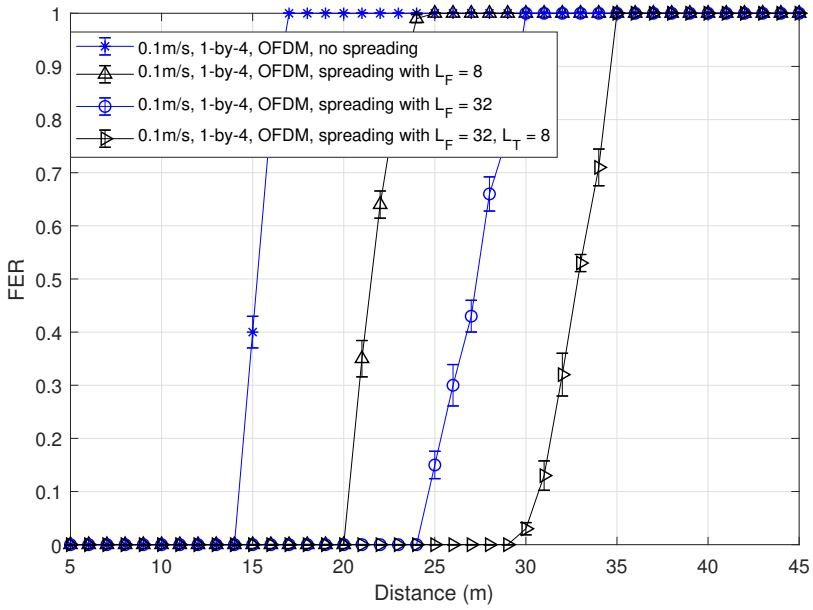

Figure 4.5: FER of 1-by-4 system with OFDM modulation when the AUV speed is $0.1\ \mathrm{m/s}$

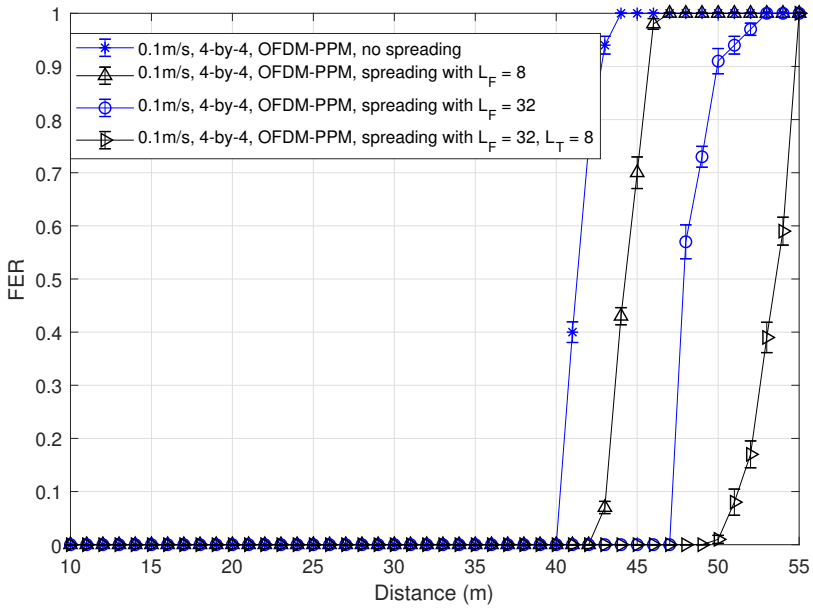

Figure 4.6: FER of 4-by-4 system with OFDM-PPM modulation when the AUV speed is $0.1\ \mathrm{m/s}$

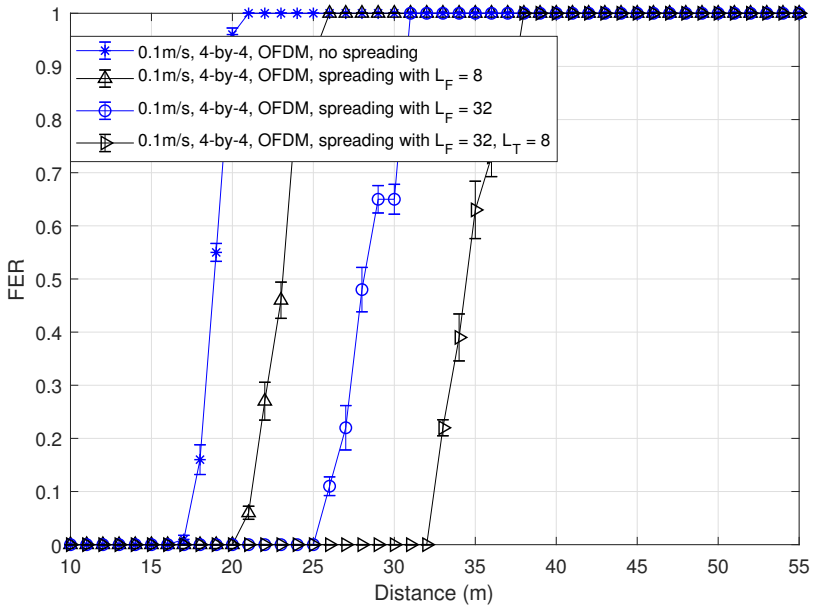

Figure 4.7: FER of 4-by-4 system with OFDM modulation when the AUV speed is $0.1\ \mathrm{m/s}$

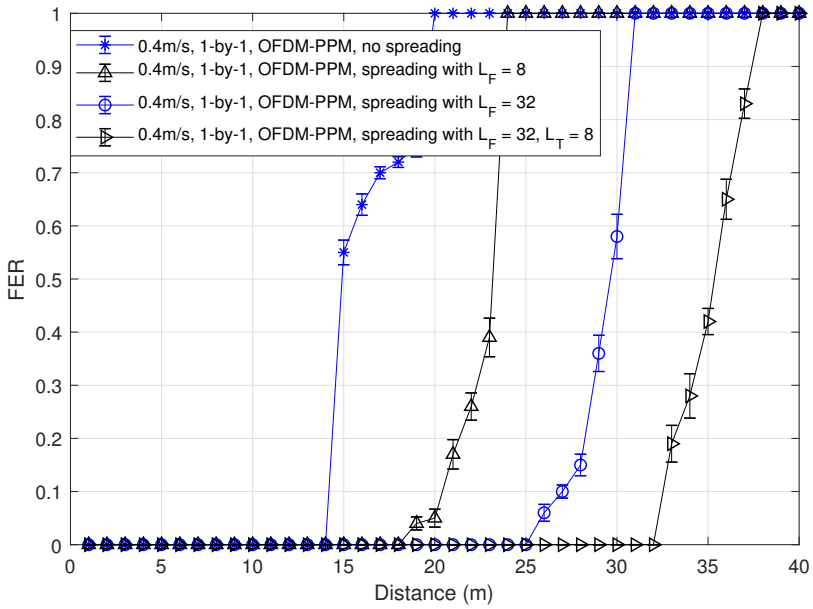

Figure 4.8: FER of 1-by-1 system with OFDM-PPM modulation when the AUV speed is $0.4\ \mathrm{m/s}$

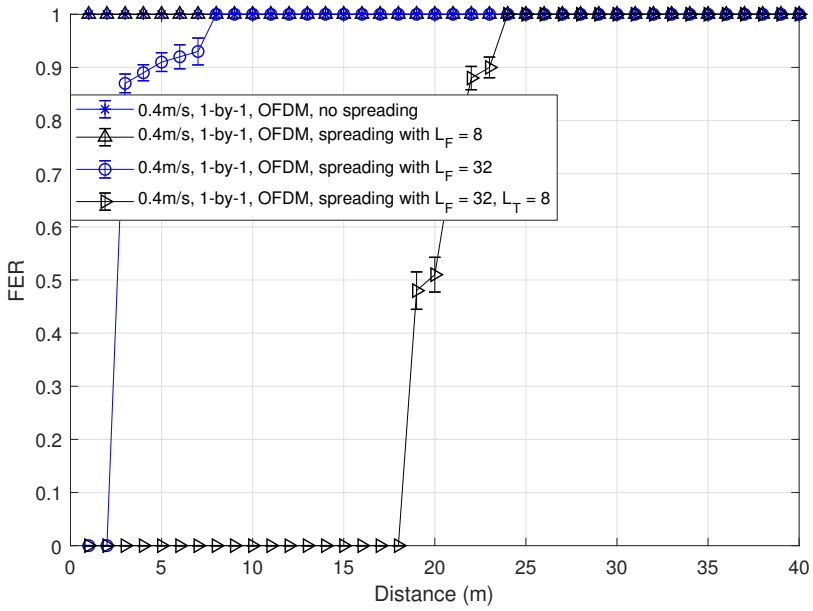

Figure 4.9: FER of 1-by-1 system with OFDM modulation when the AUV speed is $0.4\ \mathrm{m/s}$

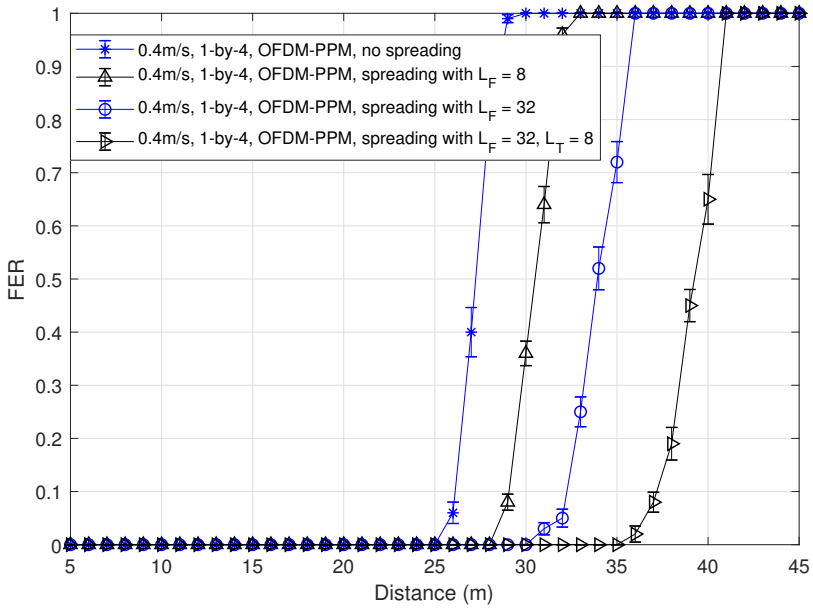

Figure 4.10: FER of 1-by-4 system with OFDM-PPM modulation when the AUV speed is $0.4\ \mathrm{m/s}$

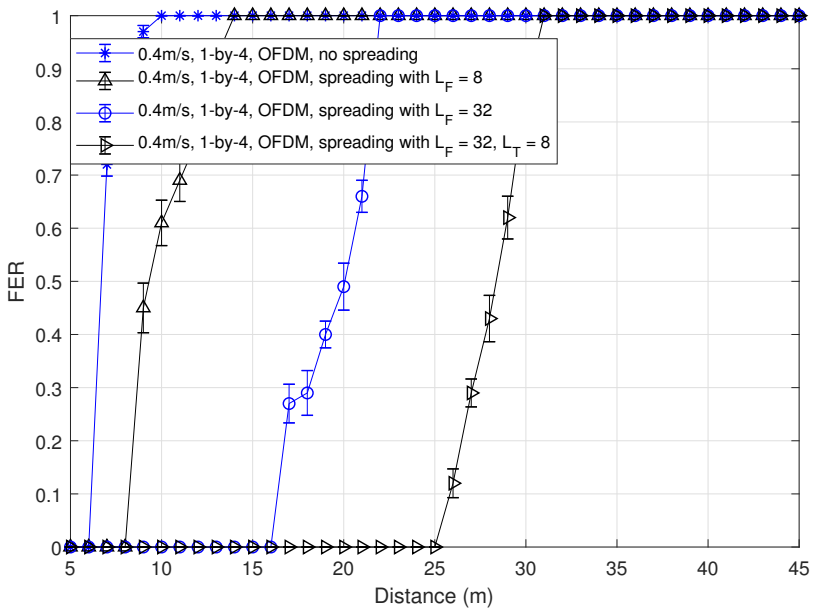

Figure 4.11: FER of 1-by-4 system with OFDM modulation when the AUV speed is $0.4\ \mathrm{m/s}$

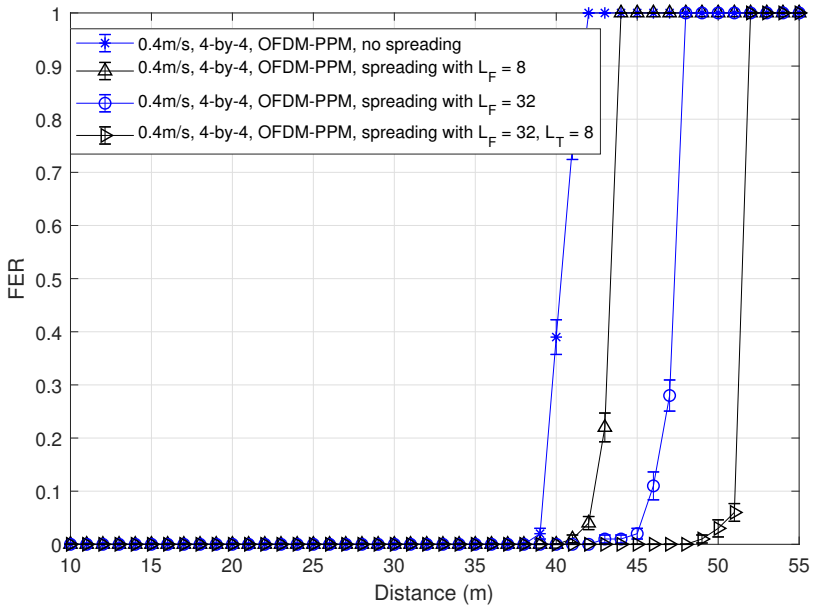

Figure 4.12: FER of 4-by-4 system with OFDM-PPM modulation when the AUV speed is $0.4\ \mathrm{m/s}$

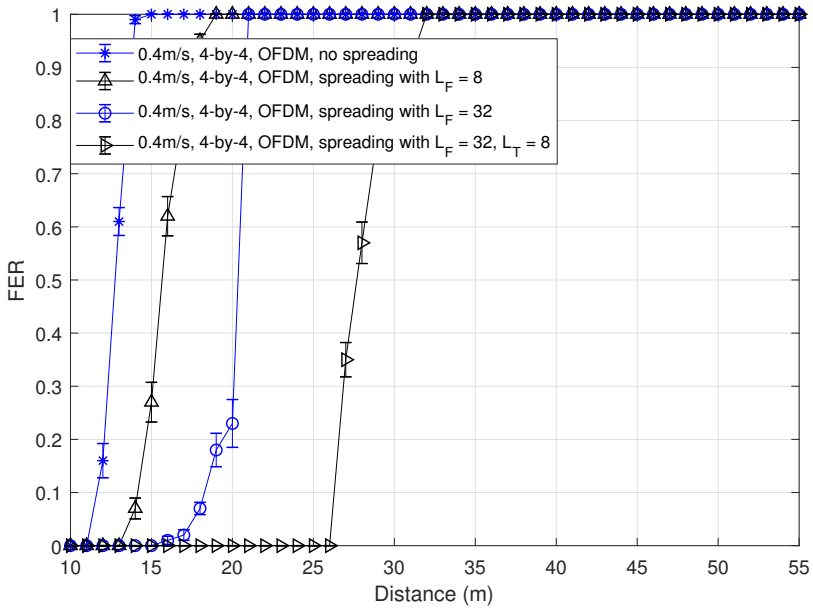

Figure 4.13: FER of 4-by-4 system with OFDM modulation when the AUV speed is $0.4\ \mathrm{m/s}$

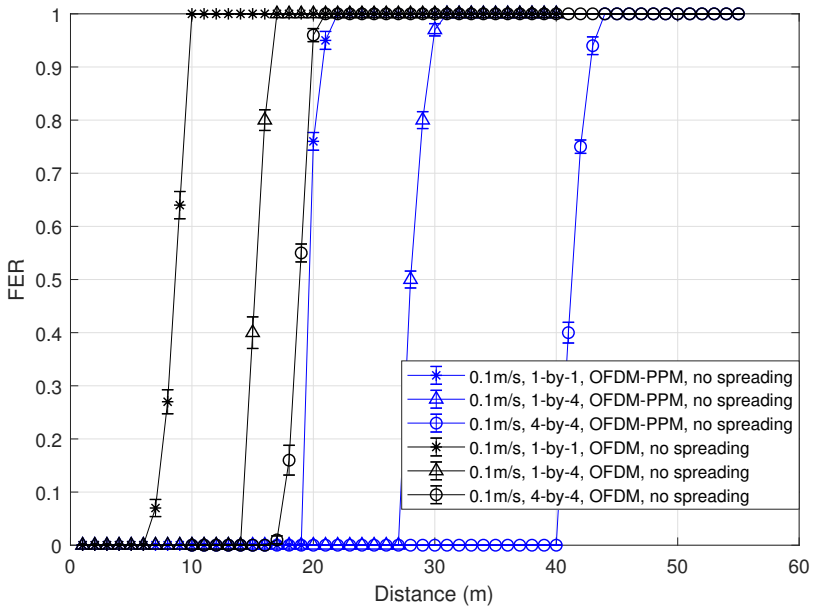

Figure 4.14: FER of without TF-spreading when the AUV speed is $0.1\ \mathrm{m/s}$

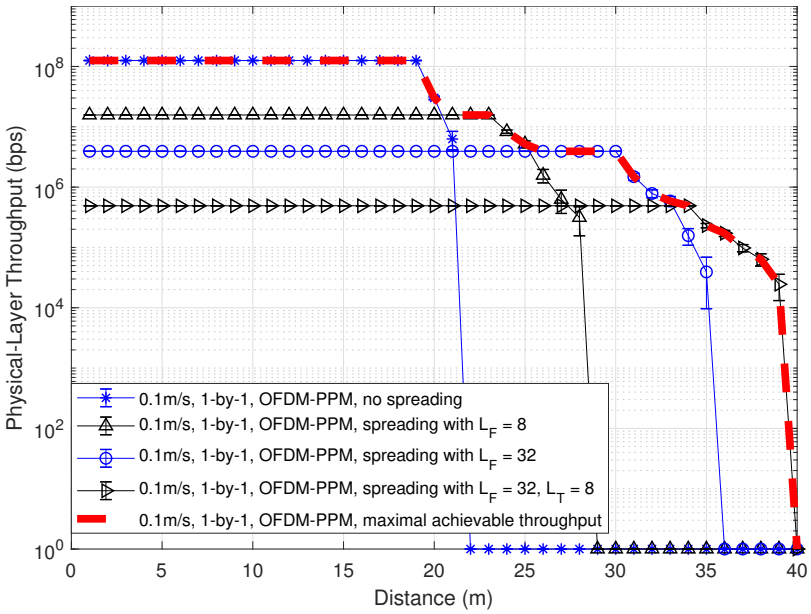

Figure 4.15: The physical-layer throughput of 1-by-1 system with OFDM-PPM modulation with an AUV speed of $0.1\ \mathrm{m/s}$

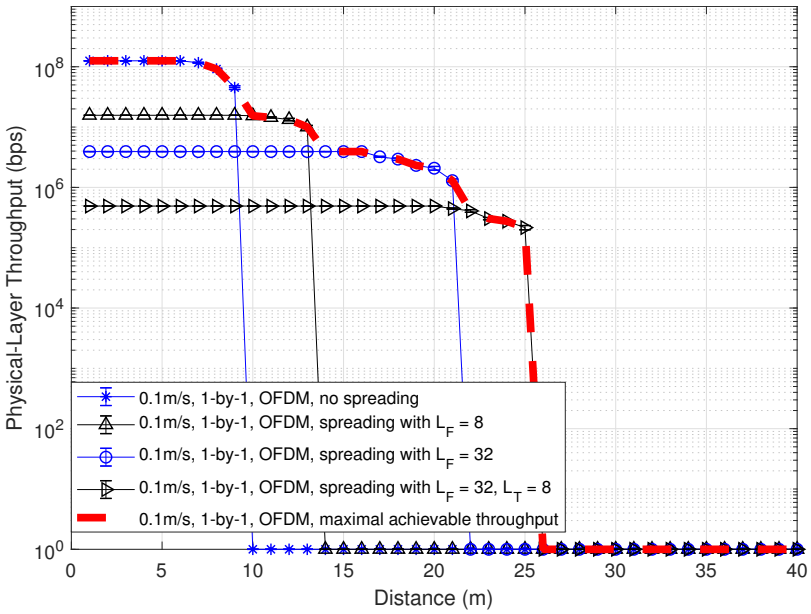

Figure 4.16: The physical-layer throughput of 1-by-1 system with OFDM modulation with an AUV speed of $0.1\ \mathrm{m/s}$

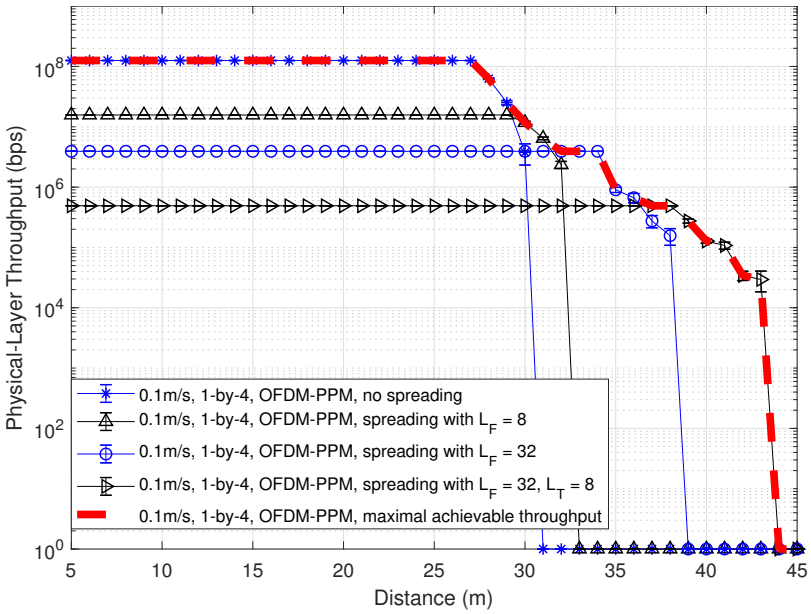

Figure 4.17: The physical-layer throughput of 1-by-4 system with OFDM-PPM modulation with an AUV speed of $0.1\ \mathrm{m/s}$

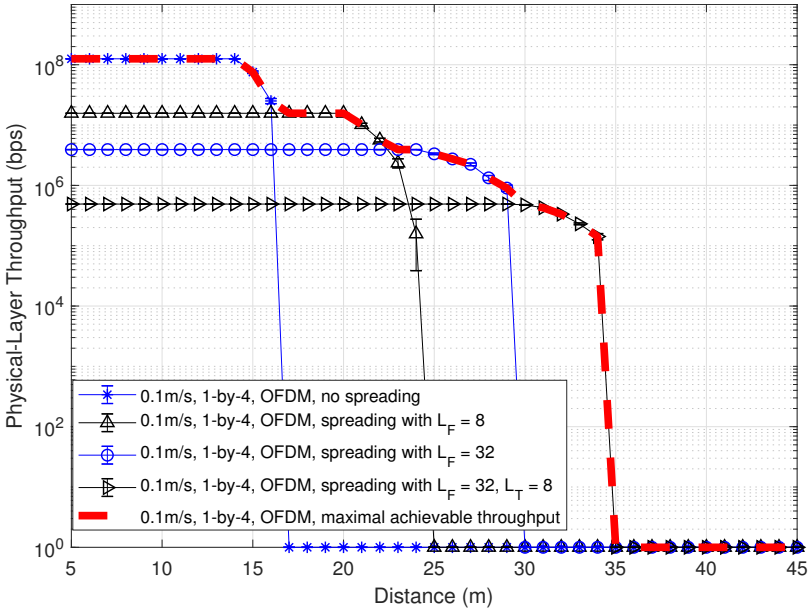

Figure 4.18: The physical-layer throughput of 1-by-4 system with OFDM modulation with an AUV speed of $0.1\ \mathrm{m/s}$

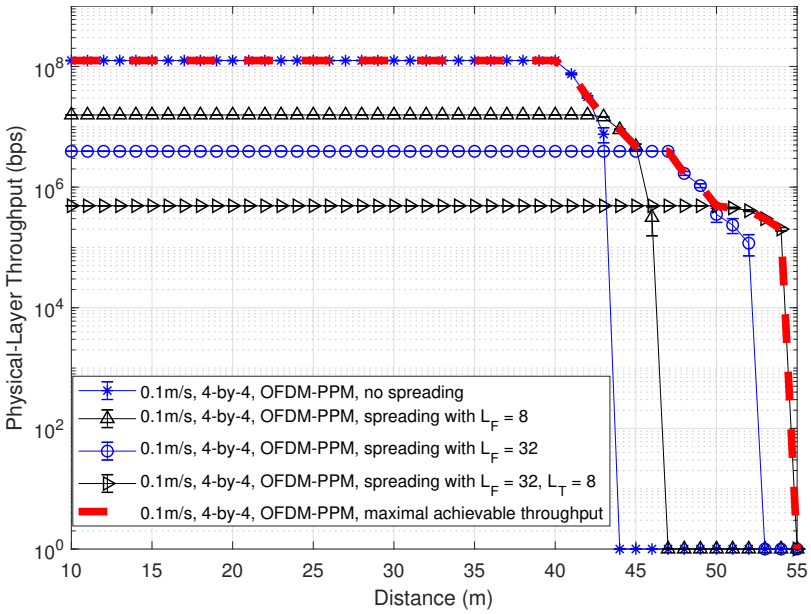

Figure 4.19: The physical-layer throughput of 4-by-4 system with OFDM-PPM modulation with an AUV speed of $0.1\ \mathrm{m/s}$

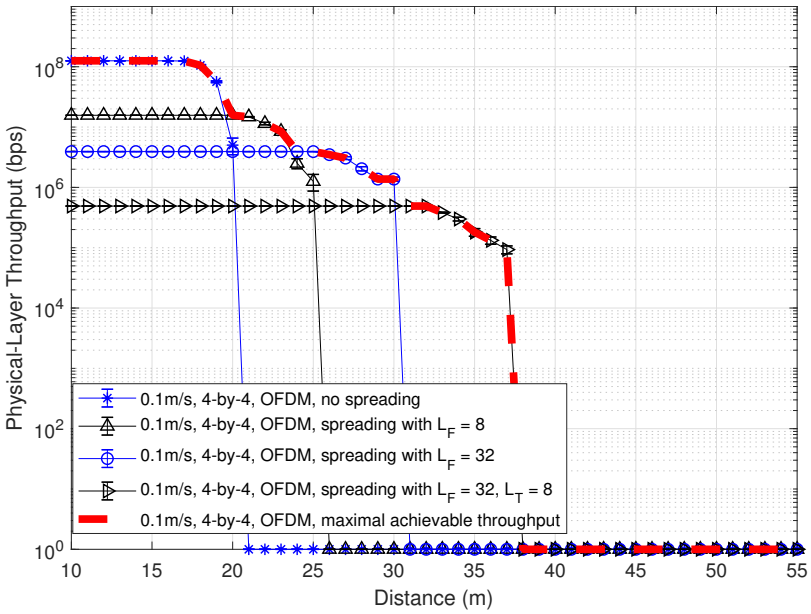

Figure 4.20: The physical-layer throughput of 4-by-4 system with OFDM modulation with an AUV speed of $0.1\ \mathrm{m/s}$

CHAPTER 5
UNDERWATER ACOUSTIC WIRELESS COMMUNICATION EXPERIMENT

To explore the properties of UAWC, we design a series of testbed-based experiments in the tank (Figure 5.1) and the pool (Figure 5.2), respectively. In our work, to detect and record acoustic signals, hydrophones and USRPs are utilized. The transmitted and received data will be processed using MATLAB. The connection of hardware for UWAC system is shown in Figure 5.3.

5.1 Hydrophones

One of the most common ways of employing UAWC is to deploy hydrophones (Figure 5.4). The underwater acoustic wave is composed of alternating compressions and rarefactions of the water. Most hydrophones are equipped with a certain ceramics, which produces small-voltage signals once subjected to changes in underwater pressure. Thus the hydrophone can measure underwater acoustic signals by recording the voltage signals from the ceramics.

A series of highly sensitive hydrophones, called RESON TC 4013, designed by TELEDYNE MARINE [61], are deployed in our research. The RESON TC 4013 offers a uniform omnidirectional sensitivity in both horizontal and vertical planes. It can work as an excellent transducer by making absolute sound measurements and calibrations with a frequency range of $170\ \mathrm{kHz}$. Moreover, it can also be deployed as an omnidirectional transmit antenna.

5.2 Universal Software Radio Peripheral

A high-performance and scalable platform (Figure 5.5), called X-310 designed by Ettus

Figure 5.1: Test in tank

Research and its parent company, National Instruments [62], is deployed in this research. It contains a large Kintex-7 FPGA which provides additional space for developers to incorporate custom digital signal processing blocks. The USRP will be connected with a host computer to transmit and receive signals. Each USRP board contains two channels and two master clock rates.

5.3 Voltage Preamplifier

A voltage preamplifier (Figure 5.6), called EC6081 mk2 (VP2000) designed by TELEDYNE MARINE [63], is deployed in conjunction with piezoelectric hydrophones. It offers excellent low-noise performance over the entire frequency range (up to 1 MHz). Besides, it provides with 1Hz to 1MHz bandwidth Gain selection and 12 high-pass and 12 low-pass

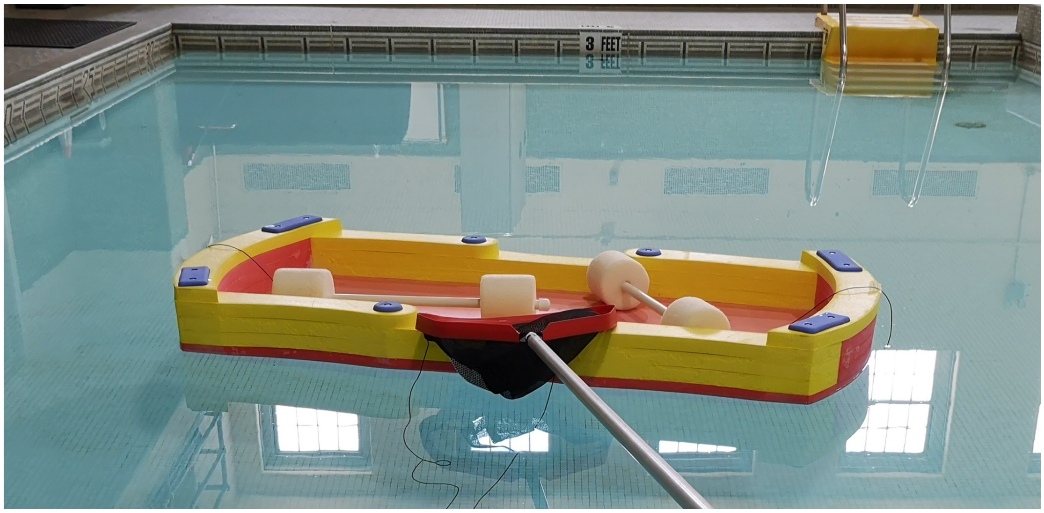

Figure 5.2: Test in pool

filters in total, which can be used for designing ideal bandpass filter.

5.4 Software

A radio-in-the-loop design and modeling environment can be provided by MATLAB by connecting to USRP software-defined radios from Ettus Research, LLC. With Communications Toolbox, the support package, and a USRP radio (X310), practical software-defined radios systems can be designed and verified [64, 65]. The support package includes functions and system objects for connecting MATLAB to USRP-Hardware-Driver-based USRP radios, such as SDRuTransmitter System object and SDRuReceiver System object.

To use the Communication Toolbox Support Package for USRP Radio features, communication between the host computer and the radio hardware is established with an Ethernet cable.

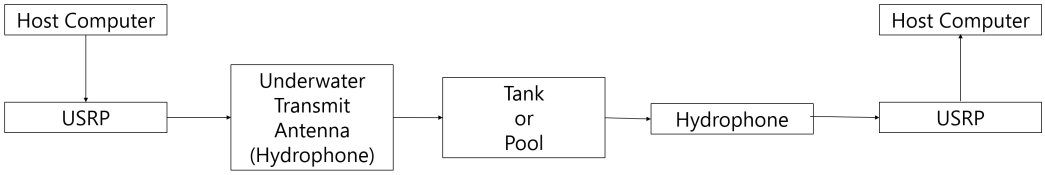

Figure 5.3: Hardware connection

5.5 experimental Design

The structure of our testbed-based UWAC system is shown in Figure 5.7. At the transmitter, we first apply the channel coding (e.g., Turbo code), then adopt the interleaving technique to place the error bits sparsely in the data sequence. Then we do the constellation mapping corresponding to the source code modulation. After baseband modulation, a S/P conversion is adopted. Then, we generate OFDM frequency-domain symbols by IFFT. The OFDM frames are composed of pilot frames and data frames. If we use ”P” to represent pilot frame and use ”D” to represent data frames, the structure of OFDM frames is [P D D P D D P ...]. After space-time coding, we process the digital signals with DAC. Then the data streams can be transmitted by transducers.

At the receiver, the time synchronization is done based on the high auto-correlation of M-sequence. After ADC, OFDM de-modulation is performed. To decode the receive data, channel estimation is needed to get the channel information. For MIMO transmission, scheme, the estimated channel is calculated by ZF. As for SIMO, Maximal Ratio Combining (MRC) is utilized to enhance the system robustness. After space-time decoding and constellation de-mapping, the de-interleaving and channel decoding are subsequently performed.

The hardware and software parameters are set in Table. 5.1. The center frequency of acoustic signals is 100 kHz. The underwater acoustic speed is about 1500 m/s. The number of transmit antennas is 1 or 2 in the tank and is 1 in the pool. The number of receive antennas is 1 or 2 in the tank and is 1 in the pool. The baseband modulation is BPSK or QPSK in the tank and is BPSK in the pool. With a wave speed of lower than

Figure 5.4: RESON TC 4013 Hydrophone [61]

Figure 5.5: USRP X310 [62]

Figure 5.6: VP2000 voltage preamplifier [63]

$0.1\ \mathrm{m/s}$, the coherence time is about $150\ \mathrm{ms}$, so OFDM FFT size is chosen to be 6144. The length of CP T_{CP} is related to the length of the OFDM symbol T_{OFDM} as $T_{OFDM} = \alpha T_{CP}$, where α is a constant. It is expected that the length of the OFDM symbol should be longer than the length of the CP. Since the propagation delay is around $10\ \mathrm{ms}$, we choose the CP length to be $10240\ \mu\mathrm{s}$ to mitigate the ISI effect. With the OFDM system bandwidth to be $100\ \mathrm{kHz}$, overall the OFDM symbol length to be $71680\ \mu\mathrm{s}$, and the subcarrier spacing to be $16.28\ \mathrm{Hz}$. FFT size and a CP length are fixed; this is because practical systems generally adopt fixed FFT size and a CP length.

5.6 Experimental Result

Figure 5.8 depicts the signal-to-noise ratio versus distance in the tank. The distance in the tank varies from $13\ \mathrm{cm}$ to $38\ \mathrm{cm}$, while the SNR varies between $40\ \mathrm{dB}$ and $44\ \mathrm{dB}$. Figures 5.9 to 5.16 depict the results of experiments in the tank, while Figures 5.18 to 5.23

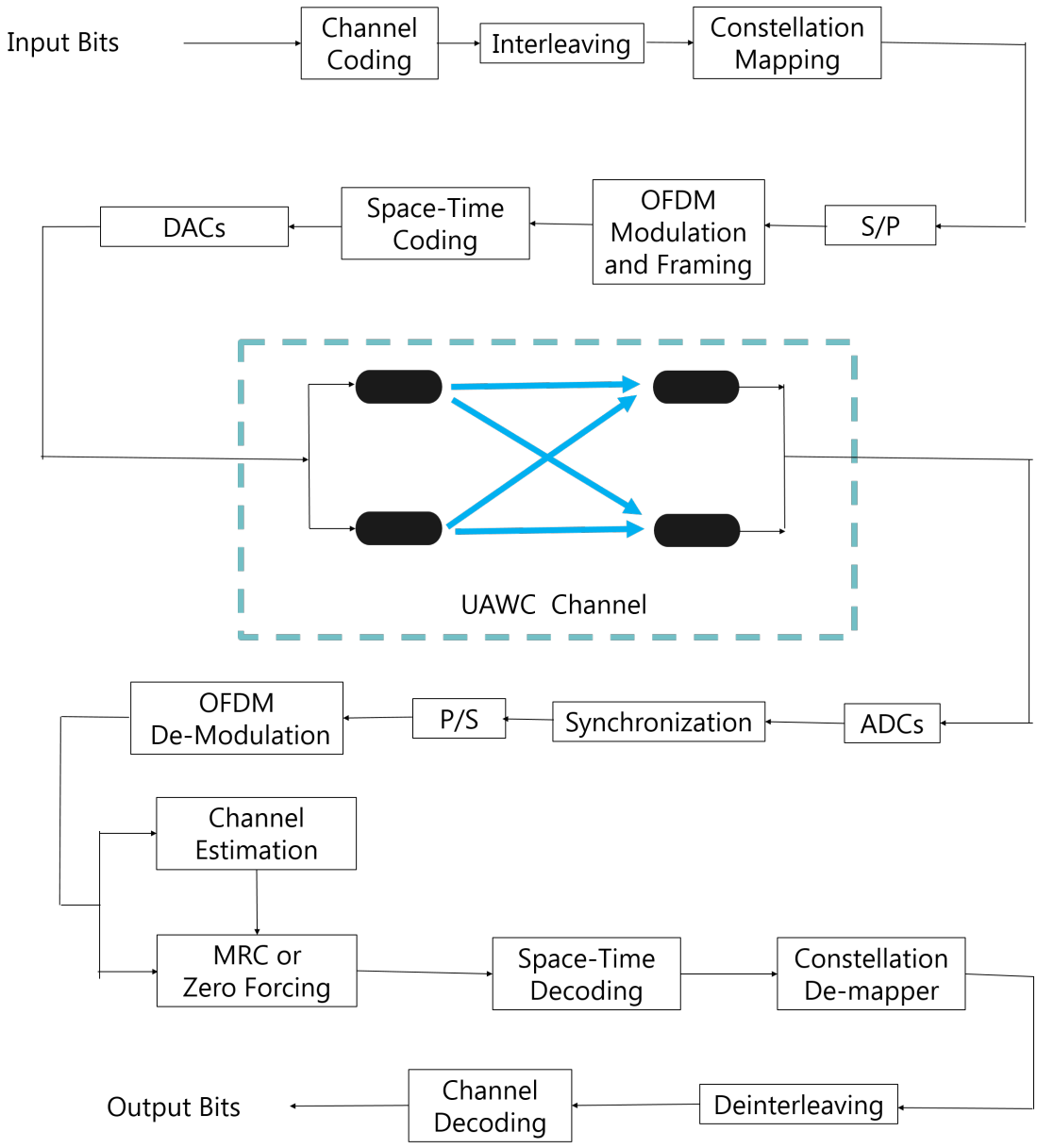

Figure 5.7: Underwater acoustic system structure

Table 5.1: UAWC Experiment Parameters.

Parameters	**Value**
Center Frequency f_c	100 kHz
Underwater Acoustic Speed v_c	1500 m/s
Number of Transmit Antennas N_R	1 or 2
Number of Hydrophones at Receiver N_T	1 or 2
Baseband Modulation	BPSK or QPSK
OFDM FFT-size K_{FFT}	6144
Length of CP T_{CP}	10240 μs
Channel Coding Rate R_{chc}	$1/3$
Time Period of OFDM Symbol T_{OFDM}	71680 μs
Output Samples Per Symbol at Transmitter	4
Iutput Samples Per Symbol at Receiver	4
Samples Per Frame of ADC at Receiver	1024
Confidence Level	95%
Tank size	51 cm (**L**) 26 cm (**W**) 32 cm (**H**)
Power Output of USRP X310	> 10 dBm
Overall Gain for the USRP Hardware Receiver Data Path	8 dB
Overall Gain for the USRP Hardware Transmitter Data Path	8 dB
Output Gain of Voltage Preamplifier	20 dB
Frequency Band of Voltage Preamplifier	$10 - 500$ kHz
Depth in Tank Experiment	6 cm
Depth in Pool Experiment	60 cm
Wave Speed	< 0.1 m/s

depict the results of experiments in the pool. The major findings of the following results include the BER variations from the increase of the distance, the physical-layer throughput variations from the distances, the transmission rate and the order of baseband modification, and the channel impulse response in the pool.

Figures 5.9, 5.11, 5.13 and 5.15 depict the BER performances of systems versus distance. For the 1-by-1 system with BPSK (Figure 5.9), the BER is 0 when the distance is shorter than $22\ \mathrm{cm}$, and the BER is lower than 0.02 when the distance is increased. For the 1-by-1 system with QPSK, the BER is 0 when the distance is shorter than $13\ \mathrm{cm}$, lower than 0.02 when the distance is between $13\ \mathrm{cm}$ and $22\ \mathrm{cm}$, and higher than 0.04 when the distance is longer than $26\ \mathrm{cm}$. It can be found that compared with BPSK, QPSK is more likely to be wrongly decoded with the same energy per symbol.

Figure 5.11 depicts the BER performance of the 1-by-2 system. For BPSK, the BER is 0 when the distance is shorter than $31\ \mathrm{cm}$, and the BER is lower than 1.4×10^{-3} when the distance is increasing. For QPSK, the BER is 0 when the distance is shorter than $22\ \mathrm{cm}$, and the BER is lower than 1.8×10^{-3} when the distance is increase. Compared with the 1-by-1 system, the coverage distance of 1-by-2 system is greatly improved, and the BER is decreased significantly. The reason why it performs like this is that spatial diversity helps improve the system robustness by offering several observations of the same signal, which mitigates the effect of a deep fading channel.

Figure 5.13 depicts the BER performance of the 2-by-2 system with STBC. The BER is 0 when the distance is shorter than $32\ \mathrm{cm}$. For QPSK, the BER is lower than 0.05 when the distance is between $13\ \mathrm{cm}$ and $22\ \mathrm{cm}$, lower than 0.1 when the distance is increased. Figure 5.15 depicts the BER performance of the 2-by-2 system with V-BLAST. The BER is between 0.2 and 0.3 when the distance is shorter than $26cm$. For QPSK, the BER is between 0.3 and 0.4 when the distance is shorter than $31\ \mathrm{cm}$. When the distance is $38\ \mathrm{cm}$, the BERs of BPSK and QPSK are almost the same, which is because the wireless link is already very bad. Compared with STBC system, V-BLAST system leads to more interference since two

different streams are transmitted simultaneously.

Figures 5.10, 5.12, 5.14 and 5.16 depict the physical-layer throughputs of systems. For the 1-by-1 system with BPSK, the achievable physical-layer throughput is about 5.7×10^4 bps. For the 1-by-1 system with QPSK, the achievable physical-layer throughput is about 11.5×10^4 bps for QPSK, which doubles the physical-layer throughput of the 1-by-1 system with BPSK. For the 1-by-2 system and 2-by-2 system with STBC, the achievable physical-layer throughputs are almost the same as that of the 1-by-1 system. For the 2-by-2 system with V-BLAST, the achievable physical-layer throughput is about 0.9×10^5 bps with BPSK, about 1.57×10^5 bps with QPSK, which almost double the achievable physical-layer throughput compared with those of 1-by-1 system, 1-by-2 system, and 2-by-2 STBC system. The reason is that multiplexing transmits different data streams with different antennas at the same time, which improves the transmission data rate.

Figures 5.18 to 5.23 depict the results of experiments in the pool, where the wave speed is lower than 0.1 m/s. The antennas are fixed in the center of the pool. Figure 5.18 depicts the BER of each frame when the distance is 25 cm, and the SNR at the receiver is 7.92 dB. It can be observed that the BER is lower than 7×10^{-5}. Figure 5.19 depicts the channel impulse response, from which we can find that the wireless link is good with low attenuation and low channel distortion. Figures 5.20 and 5.22 depict the BER of each frame when the distance is 4.57 m and the SNR at the receiver is 1.32 dB and 1.20 dB. We can observe that the BER is equal to 0 at most time, but errors occur randomly and suddenly with BER up to 0.45. Figures 5.21 and 5.23 depict the channel impulse responses with a distance of 4.57 m. We can find that the attenuation increases significantly compared with that when the distance is 25 cm. In addition, compared with the channel impulse response in the tank (Figure 5.17), the channel in the pool has less multipath.

In this chapter, we introduce the hardware equipment and experimental structure. The experiments are done in the tank and pool, respectively. It is proven that the OFDM works underwater acoustic environment. As for the transmission schemes, the spatial diversity

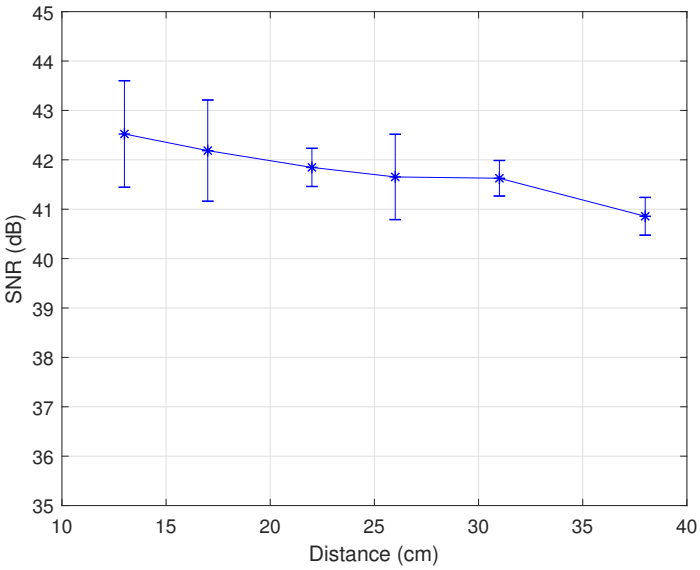

Figure 5.8: SNR at the receiver in the tank

works in improving system robustness and coverage distance, while the spatial multiplexing helps to enhance the transmission data rate.

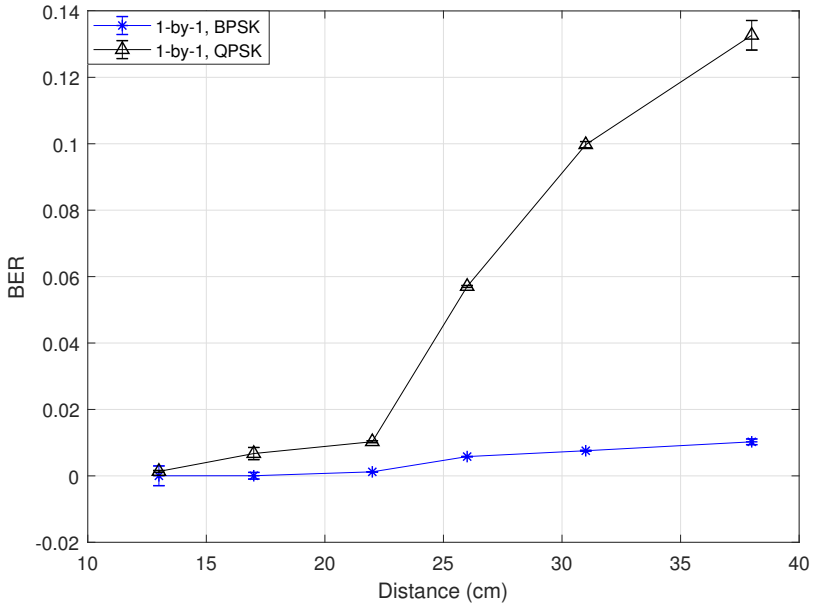

Figure 5.9: BER of 1-by-1 UAWC

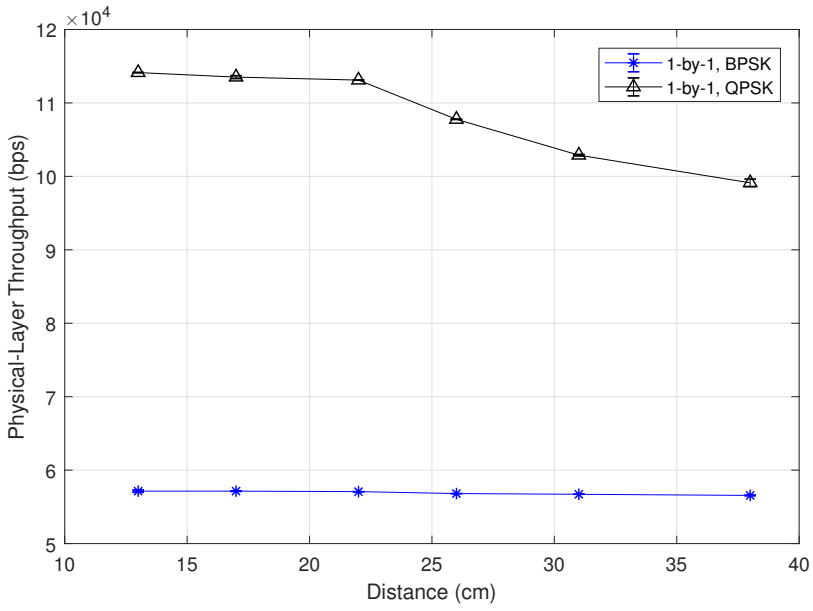

Figure 5.10: Physical-layer throughput of 1-by-1 UAWC

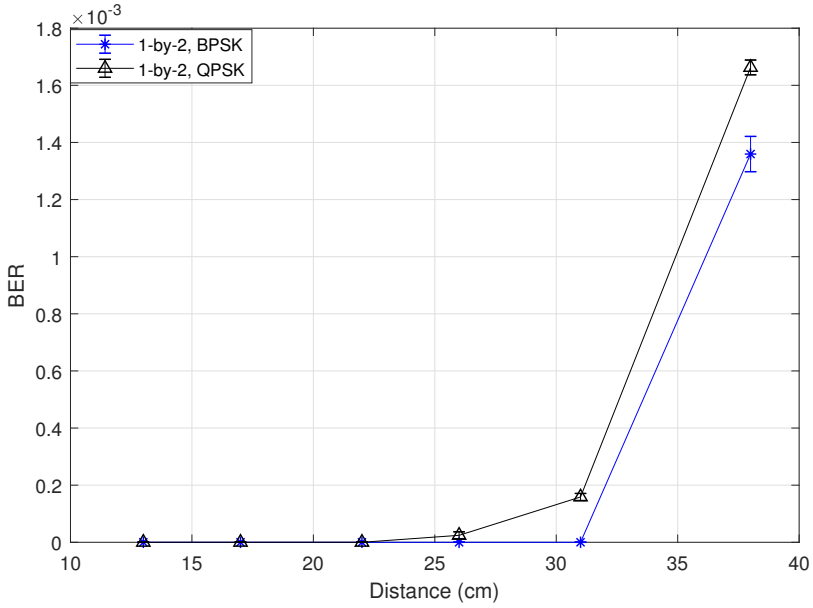

Figure 5.11: BER of 1-by-2 UAWC

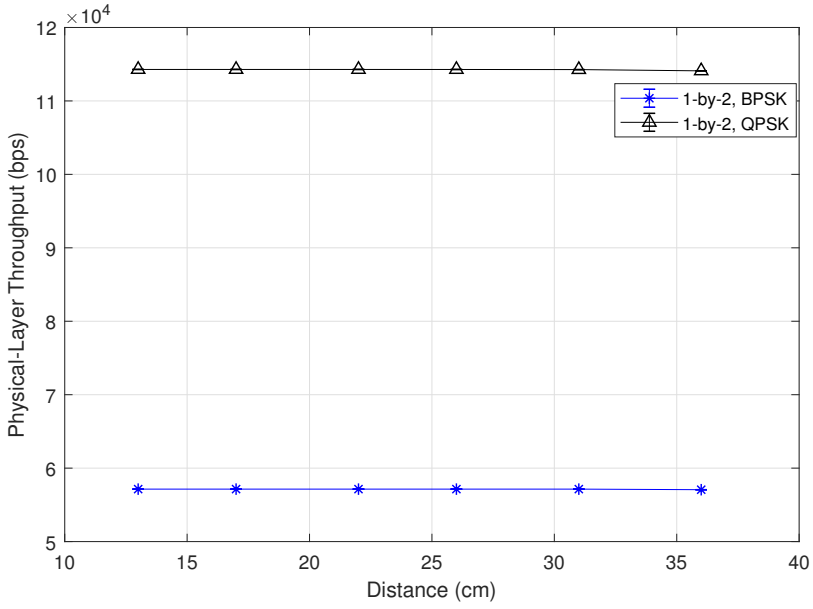

Figure 5.12: Physical-layer throughput of 1-by-2 UAWC

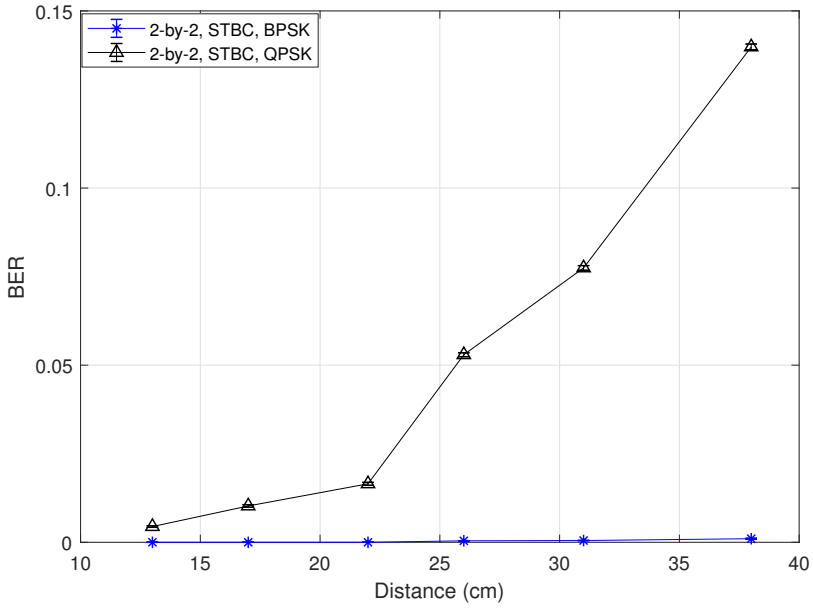

Figure 5.13: BER of 2-by-2 UAWC with STBC

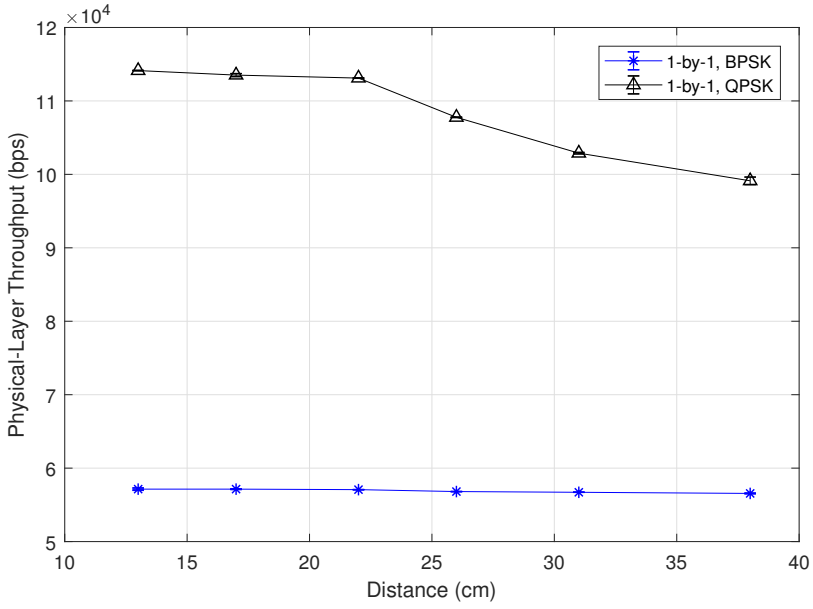

Figure 5.14: Physical-layer throughput of 2-by-2 UAWC with STBC

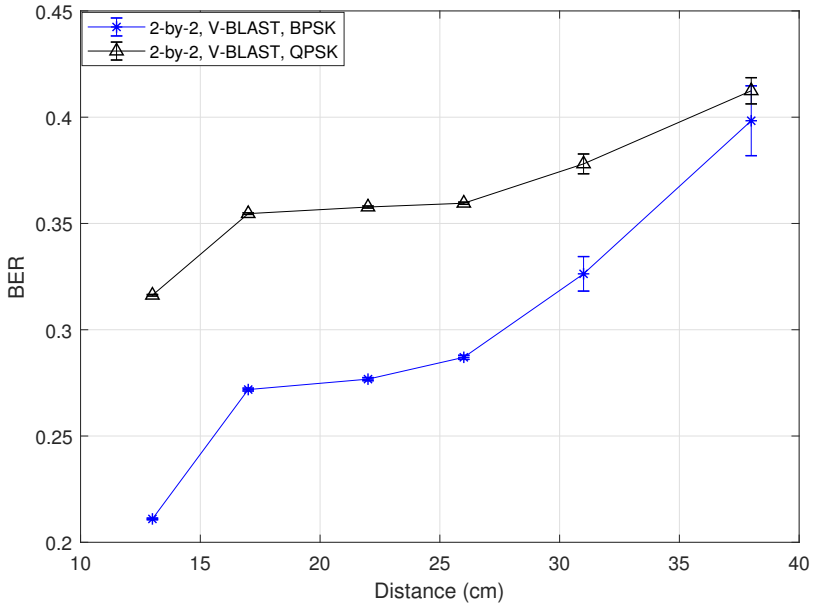

Figure 5.15: BER of 2-by-2 UAWC with V-BLAST

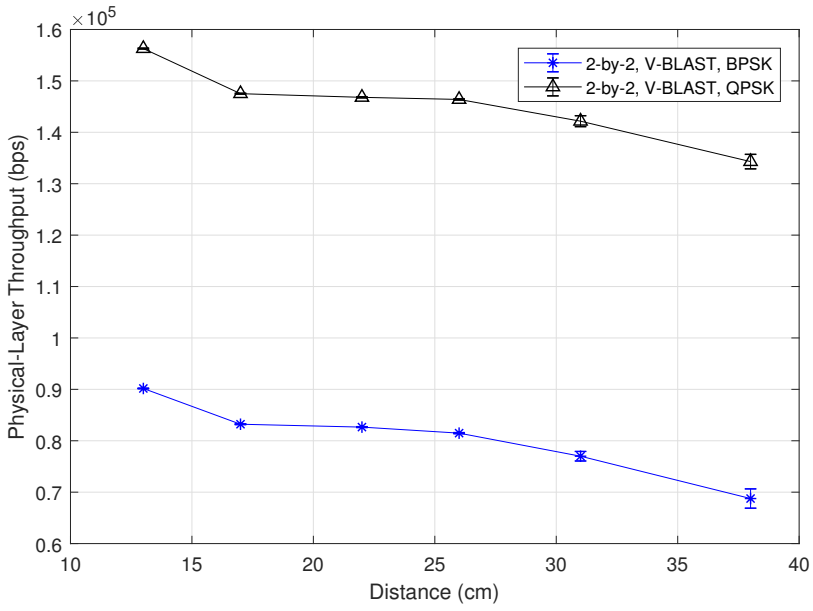

Figure 5.16: Physical-layer throughput of 2-by-2 UAWC with V-BLAST

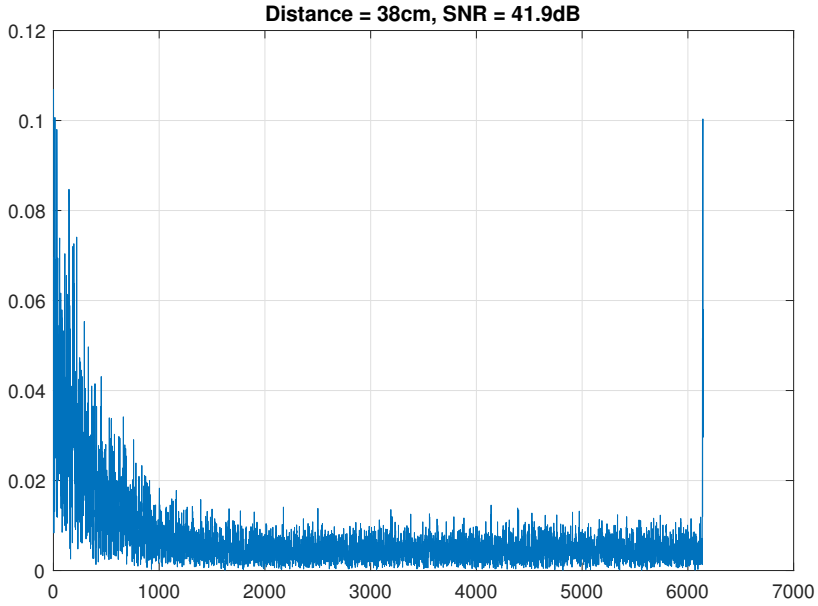

Figure 5.17: Channel impulse response in tank

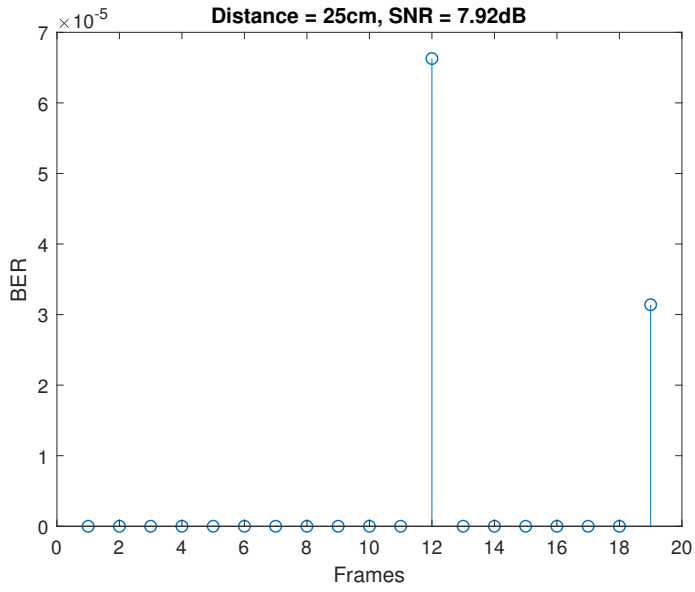

Figure 5.18: BER of 1-by-1 UAWC with a distance of 25 cm and $SNR = 7.92$ dB

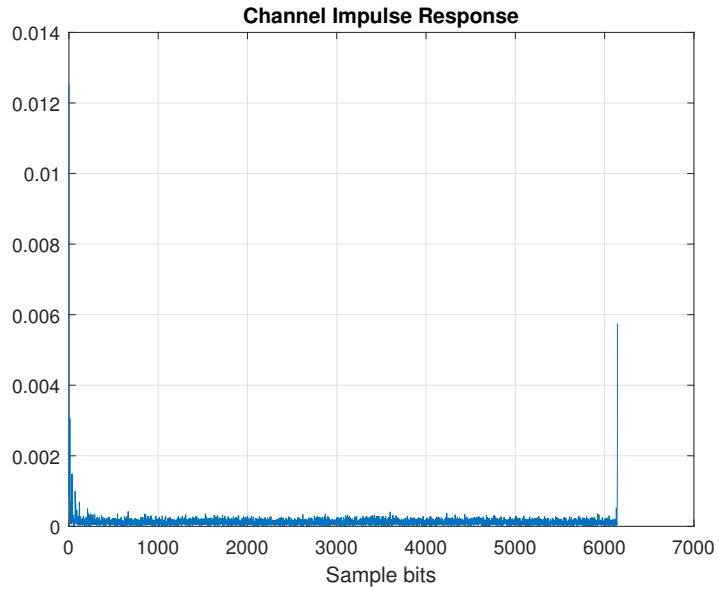

Figure 5.19: Channel impulse response of 1-by-1 UAWC with a distance of 25 cm and $SNR = 7.92$ dB

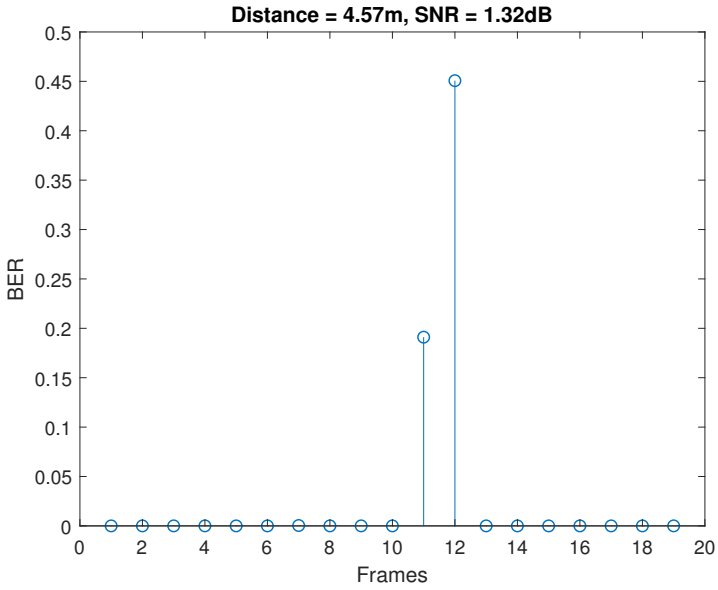

Figure 5.20: BER of 1-by-1 UAWC with a distance of 4.57 m and $SNR = 1.32$ dB

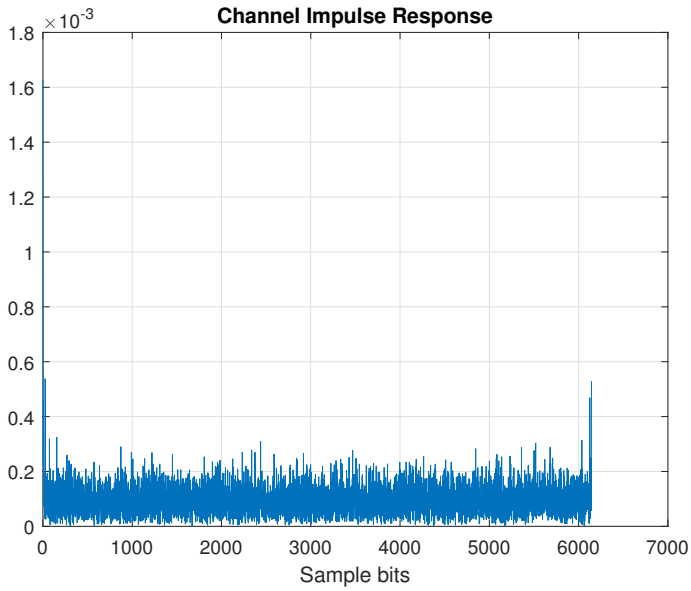

Figure 5.21: Channel impulse response of 1-by-1 UAWC with a distance of 4.57 m and $SNR = 1.32$ dB

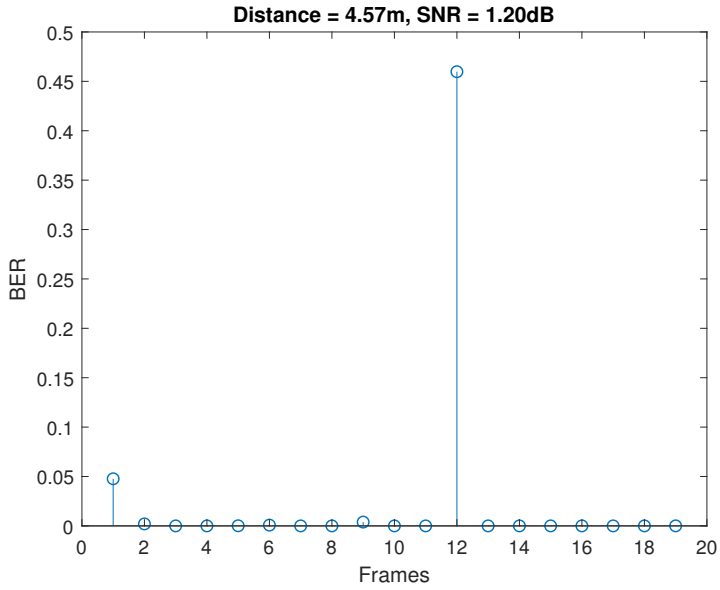

Figure 5.22: BER of 1-by-1 UAWC with a distance of 4.57 m and $SNR = 1.20$ dB

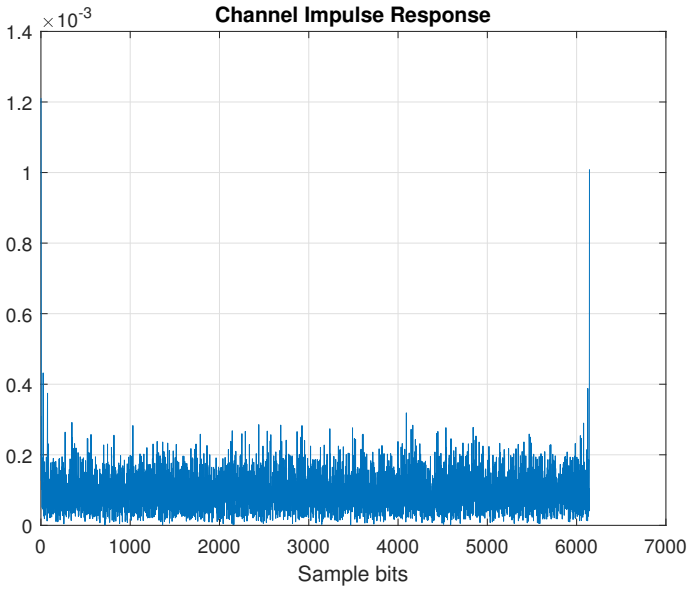

Figure 5.23: Channel impulse response of 1-by-1 UAWC with a distance of 4.57 m and $SNR = 1.20$ dB

CHAPTER 6
CONCLUSION AND FUTURE WORK

A new physical-layer system architecture for UOWC is proposed in this thesis. The motivation for this new architecture is to improve the coverage significantly. The key feature of the proposed architecture is the integration of the hybrid OFDM-PPM modulation and TF-spreading into the whole physical-layer framework. The architecture is realized by the physical-layer simulator and is further validated under realistic underwater optical channel modeling. Results indicate that the proposed hybrid PPM-OFDM with spatial diversity can improve the coverage distance by several folds compared with ordinary OFDM setups. TF-spreading improves the coverage distance by creating SNR gain, while the physical-layer throughput is decreased with the increase of the length of TF-spreading. The spatial diversity also helps to improve the coverage distance by enhancing the robustness of wireless communication link. And the issue of Doppler effect can be solved effectively with the utilization of hybrid OFDM-PPM modulation technique and TF-spreading.

In addition, the OFDM modulation has been proven in UAWC for SISO, SIMO, and MIMO system. The increase of the order of baseband modulation will lead to higher BER but will improve the transmission data rate as well as the physical-layer throughput. The spatial diversity will enhance the robustness of wireless link and decrease the BER. Spatial multiplexing will increase the transmission data rate and physical-layer throughput, but increase the BER as a trade-off. Comparing the channel impulse responses in the tank and the pool, we can find that the transmission in the tank suffers more multipath delay.

As future work, the maximum tolerable clock drift needs to be improved, and a synchronization scheme for hybrid PPM-OFDM will be explored. An optical testbed will be deployed to validate the proposal and the models used in simulations. Moreover, UAWC with more transmission schemes will be tested. The number of transmit and receive anten-

nas will be increased. To extend the coverage distance, the amplifiers will be introduced to the transmitter. To mitigate the effect of fading channel, new pilot constructs and channel estimation and equalization scheme will be explored. Notice that there is a trade-off between distance and physical-layer throughput with different transmission scheme, the adaptive transmission modulation scheme will be studied. Furthermore, an adaptive scheme for underwater communications will be under research, namely underwater acoustic-optical wireless communication, which aims to realize the switch between UAWC and UOWC with optimal choices. With this adaptive transmission scheme, it will switch to UOWC in short distances for higher transmission data rate, and switch to UAWC when long distances are in need.

REFERENCES

[1] W. Weisler, W. Stewart, M. B. Anderson, K. J. Peters, A. Gopalarathnam, and M. Bryant, "Testing and characterization of a fixed wing cross-domain unmanned vehicle operating in aerial and underwater environments," *IEEE Journal of Oceanic Engineering*, vol. 43, no. 4, pp. 969–982, 2018.

[2] M. Sasano, S. Inaba, A. Okamoto, T. Seta, K. Tamura, T. Ura, S. Sawada, and T. Suto, "Development of a regional underwater positioning and communication system for control of multiple autonomous underwater vehicles," in *2016 IEEE/OES Autonomous Underwater Vehicles (AUV)*, 2016, pp. 431–434.

[3] *Communication with submarines - Wikipedia*.

[4] S. Jaruwatanadilok, "Underwater wireless optical communication channel modeling and performance evaluation using vector radiative transfer theory," *IEEE Journal on Selected Areas in Communications*, vol. 26, no. 9, pp. 1620–1627, 2008.

[5] M. Stojanovic and J. Preisig, "Underwater acoustic communication channels: Propagation models and statistical characterization," *IEEE Communications Magazine*, vol. 47, no. 1, pp. 84–89, 2009.

[6] H. Kaushal and G. Kaddoum, "Underwater optical wireless communication," *IEEE Access*, vol. 4, pp. 1518–1547, 2016.

[7] B. Li, S. Zhou, M. Stojanovic, L. Freitag, and P. Willett, "Multicarrier communication over underwater acoustic channels with nonuniform Doppler shifts," *IEEE Journal of Oceanic Engineering*, vol. 33, no. 2, pp. 198–209, 2008.

[8] J. Xu, Y. Song, X. Yu, A. Lin, M. Kong, J. Han, and N. Deng, "Underwater wireless transmission of high-speed QAM-OFDM signals using a compact red-light laser," *Optics Express*, vol. 24, no. 8, pp. 8097–8109, 2016.

[9] H. Oubei, J. Duran, B. Janjua, H. Y. Wang, C. T. Tsai, Y. C. Chi, T. K. Ng, H. C. Kuo, J. H. He, M. S. Alouini, G. R. Lin, and B. Ooi, "4.8 Gbit/s 16-QAM-OFDM transmission based on compact 450-nm laser for underwater wireless optical communication," *Optics Express*, vol. 23, no. 18, pp. 23 302–23 309, 2015.

[10] M. Doniec, M. Angermann, and D. Rus, "An end-to-end signal strength model for underwater optical communications," *IEEE Journal of Oceanic Engineering*, vol. 38, no. 4, pp. 743–757, 2013.

[11] M. Rahmati and D. Pompili, "uwMIMO-HARQ: Hybrid ARQ for reliable underwater acoustic MIMO communications," in *Proceedings of the 10th International Conference on Underwater Networks & Systems (WUWNet '15)*, Arlington, VA, USA, 2015, 12:1–12:8.

[12] X. Zhao and D. Pompili, "AMMCA: Acoustic massive MIMO with carrier aggregation to boost the underwater communication data rate," in *10th ACM International Conference on Underwater Networks and Systems (WUWNet '15)*, 2015.

[13] X. Zhao, D. Pompili, and J. Alves, "Energy-efficient OFDM bandwidth selection for underwater acoustic carrier aggregation systems," in *2016 IEEE Third Underwater Communications and Networking Conference (UComms)*, 2016, pp. 1–5.

[14] X. Zhao, D. Pompili, and J. Alves, "Underwater acoustic carrier aggregation: Achievable rate and energy-efficiency evaluation," *IEEE Journal of Oceanic Engineering*, vol. 42, no. 4, pp. 1035–1048, 2017.

[15] M. Rahmati, A. Gurney, and D. Pompili, "Adaptive underwater video transmission via software-defined MIMO acoustic modems," in *OCEANS 2018 MTS/IEEE Charleston*, 2018, pp. 1–6.

[16] P. J. Bouvet, Y. Auffret, A. Loussert, P. Tessot, G. Janvresse, and R. Bourdon, "MIMO underwater acoustic channel characterization based on a remotely operated experimental platform," in *IEEE OCEANS*, 2014, pp. 1–6.

[17] F., R. Xu, Y. Zhang, H. Sun, and D. Wang, "Design and test of a carrier interferometry OFDM system in underwater acoustic channels," in *2008 International Conference on Communications, Circuits and Systems*, 2008, pp. 148–152.

[18] X. Zhu, Z. Xie, S. Xiong, H. Zhang, and Z. Yue, "Research on high speed OFDM underwater acoustic communication based on TPC," in *2017 IEEE International Conference on Signal Processing, Communications and Computing (ICSPCC)*, 2017, pp. 1–6.

[19] E. V. Zorita and M. Stojanovic, "Space-frequency block coding for underwater acoustic communications," *IEEE Journal of Oceanic Engineering*, vol. 40, no. 2, pp. 303–314, 2015.

[20] Y. Zhang, H. Sun, F. Xu, and D. Wang, "OFDM transform-domain channel estimation based on MMSE for underwater acoustic channels," in *2008 2nd International Conference on Anti-counterfeiting, Security and Identification*, 2008, pp. 177–181.

[21] J. Huang, J. Sun, C. He, X. Shen, and Q. Zhang, "High-speed underwater acoustic communication based on OFDM," in *2005 IEEE International Symposium on*

Microwave, Antenna, Propagation and EMC Technologies for Wireless Communications, vol. 2, 2005, 1135–1138 Vol. 2.

[22] B. Li, S. Zhou, J. Huang, and P. Willett, "Scalable OFDM design for underwater acoustic communications," in *2008 IEEE International Conference on Acoustics, Speech and Signal Processing*, 2008, pp. 5304–5307.

[23] B. Li, J. Huang, S. Zhou, K. Ball, M. Stojanovic, L. Freitag, and P. Willett, "MIMO-OFDM for high-rate underwater acoustic communications," *IEEE Journal of Oceanic Engineering*, vol. 34, no. 4, pp. 634–644, 2009.

[24] I. Nelson, K. Vishvaksenan, and V. Rajendran, "Performance of Turbo coded MIMO-OFDM system for underwater communications," in *International Conference on Communications and Signal Processing (ICCSP)*, 2014, pp. 1735–1739.

[25] K. Pelekanakis and A. Baggeroer, "Exploiting space-time-frequency diversity with MIMO-OFDM for underwater acoustic communications," *IEEE Journal of Oceanic Engineering*, vol. 36, no. 4, pp. 502–513, 2011.

[26] L. Na, H. Sun, X. Kuai, C. Ken, and Q. Jie, "Impulse noise and large scale single frequency noise mitigation for underwater acoustic OFDM," in *OCEANS 2014 - TAIPEI*, 2014, pp. 1–4.

[27] H. Sun, W. Shen, Z. Wang, S. Zhou, X. Xu, and Y. Chen, "Joint carrier frequency offset and impulse noise estimation for underwater acoustic OFDM with null subcarriers," in *2012 Oceans*, 2012, pp. 1–4.

[28] P. Zhu, X. Xu, X. Zhang, R. Wang, and X. Zhang, "A new variable step-size LMS algorithm for application to underwater acoustic channel equalization," in *2017 IEEE International Conference on Signal Processing, Communications and Computing (ICSPCC)*, 2017, pp. 1–4.

[29] W. Shen, H. Sun, E. Cheng, W. Su, and Y. Zhang, "Narrowband interference suppression in underwater acoustic OFDM system," in *2010 2nd International Asia Conference on Informatics in Control, Automation and Robotics (CAR 2010)*, vol. 1, 2010, pp. 496–499.

[30] X. Ma, C. Zhao, and G. Qiao, "The underwater acoustic OFDM channel equalizer basing on least mean square adaptive algorithm," in *2008 IEEE International Symposium on Knowledge Acquisition and Modeling Workshop*, 2008, pp. 1052–1055.

[31] L. Liu, H. Zhao, L. Zhou, J. Jin, J. Zhang, and Z. Lv, "PN sequence based underwater acoustic orthogonal signal-division multiplex communication system," in *2018 IEEE International Conference on Signal Processing, Communications and Computing (ICSPCC)*, 2018, pp. 1–6.

[32] W. Feng, X. Xu, L. Zhang, and Y. Chen, "A frame synchronization method for underwater acoustic communication on mobile platform," in *2010 International Conference on Image Analysis and Signal Processing*, 2010, pp. 518–522.

[33] Y. Xie, X. Hu, J. Xiao, D. Wang, and W. Lei, "Implementation of timing synchronization for OFDM underwater communication system on FPGA," in *2009 3rd International Conference on Anti-counterfeiting, Security, and Identification in Communication*, 2009, pp. 568–570.

[34] W. Wei, X. Hu, D. Wang, R. Xu, and H. Sun, "Performance comparison of time synchronization algorithms for OFDM underwater communication system," in *2007 14th International Conference on Mechatronics and Machine Vision in Practice*, 2007, pp. 104–107.

[35] H. M. Oubei, X. Sun, T. K. Ng, O. Alkhazragi, M. S. Alouini, and S. B. Ooi, "Scintillations of RGB laser beams in weak temperature and salinity-induced oceanic turbulence," in *2018 Fourth Underwater Communications and Networking Conference (UComms)*, 2018, pp. 1–4.

[36] P. McGillivary, V. Chirayath, and J. Baghdady, "Use of multi-spectral high repetition rate LED systems for high bandwidth underwater optical communications, and communications to surface and aerial systems," in *2018 Fourth Underwater Communications and Networking Conference (UComms)*, 2018, pp. 1–5.

[37] I. C. Lu and Y. L. Liu, "205 Mb/s LED-based underwater optical communication employing OFDM modulation," in *2018 OCEANS - MTS/IEEE Kobe Techno-Oceans (OTO)*, 2018, pp. 1–4.

[38] J. Xu, A. Lin, X. Yu, Y. Song, M. Kong, F. Qu, J. Han, W. Jia, and N. Deng, "Underwater laser communication using an OFDM-modulated 520-nm laser diode," *IEEE Photonics Technology Letters*, vol. 28, no. 20, pp. 2133–2136, 2016.

[39] C. M. Ho, C. K. Lu, H. H. Lu, S. J. Huang, M. T. Cheng, Z. Y. Yang, and X. Y. Lin, "A 10m/10Gbps underwater wireless laser transmission system," in *2017 Optical Fiber Communications Conference and Exhibition (OFC)*, 2017, pp. 1–3.

[40] H. H. Lu, C. Y. Li, H. H. Lin, W. S. Tsai, C. A. Chu, and B. R. C. amd Chang-Jen Wu, "An 8m/9.6Gbps underwater wireless optical communication system," *IEEE Photonics Journal*, vol. 8, no. 5, pp. 1–7, 2016.

[41] X. Hong, C. Fei, G. Zhang, and S. He, "Probabilistically shaped 256-QAM-OFDM transmission in underwater wireless optical communication system," in *2019 Optical Fiber Communications Conference and Exhibition (OFC)*, 2019, pp. 1–3.

[42] I. Mizukoshi, N. Kazuhiko, and M. Hanawa, "Underwater optical wireless transmission of 405nm, 968Mbit/s optical IM/DD-OFDM signals," in *2014 OptoElectronics and Communication Conference and Australian Conference on Optical Fibre Technology*, 2014, pp. 216–217.

[43] A. Huang, L. Tao, and Q. Jiang, "BER performance of underwater optical wireless MIMO communications with spatial modulation under weak turbulence," in *2018 OCEANS - MTS/IEEE Kobe Techno-Oceans (OTO)*, 2018, pp. 1–5.

[44] Y. Dong, J. Liu, and H. Zhang, "On capacity of 2-by-2 underwater wireless optical MIMO channels," in *Advances in Wireless and Optical Communications (RTUWO)*, 2015, pp. 219–222.

[45] H. Zhang, Y. Dong, and L. Hui, "On capacity of downlink underwater wireless optical MIMO systems with random sea surface," *IEEE Communications Letters*, vol. 19, no. 12, pp. 2166–2169, 2015.

[46] M. V. Jamali, J. Salehi, and F. Akhoundi, "Performance studies of underwater wireless optical communication systems with spatial diversity: MIMO scheme," *IEEE Transactions on Communications*, vol. 65, no. 3, pp. 1176–1192, 2017.

[47] H. Zhang and Y. Dong, "Impulse response modeling for general underwater wireless optical MIMO links," *IEEE Communications Magazine*, vol. 54, no. 2, pp. 56–61, 2016.

[48] C. Li, B. Wang, P. Wang, Z. Xu, Q. Yang, and S. Yu, "Generation and transmission of 745mb/s OFDM signal using a single commercial blue LED and an analog post-equalizer for underwater optical wireless communications," in *2016 Asia Communications and Photonics Conference (ACP)*, 2016, pp. 1–3.

[49] R. Qadar, M. K. Kasi, S. Ayub, and F. A. Kakar, "An adaptive approach for estimation of an underwater optical channel using Monte Carlo," in *OCEANS 2017 - Aberdeen*, 2017, pp. 1–6.

[50] W. Liu, D. Zou, Z. Xu, and J. Yu, "Non-line-of-sight scattering channel modeling for underwater optical wireless communication," in *2015 IEEE International Conference on Cyber Technology in Automation, Control, and Intelligent Systems (CYBER)*, 2015, pp. 1265–1268.

[51] J. V. Aravind, S. Kumar, and S. Prince, "Mathematical modelling of underwater wireless optical channel," in *2018 International Conference on Communication and Signal Processing (ICCSP)*, 2018, pp. 0776–0780.

[52] E. Herji, P. Andre, J. Gomes, P. Gois, and A. Pascoal, "A study of modulation formats for the blue ray underwater optical modem," in *2018 Fourth Underwater Communications and Networking Conference (UComms)*, 2018, pp. 1–5.

[53] Z. Wang, Y. Dong, X. Zhang, and S. Tang, "Adaptive modulation schemes for underwater wireless optical communication systems," in *Proceedings of the Seventh ACM International Conference on Underwater Networks and Systems (WUWNet '12)*, Los Angeles, California, 2012, pp. 1–2.

[54] X. Zhang, Y. Dong, and S. Tang, "Polarization differential pulse position modulation," in *Proceedings of the Seventh ACM International Conference on Underwater Networks and Systems (WUWNet '12)*, Los Angeles, California, 2012, pp. 1–2.

[55] H. S. Khallaf, H. M. H. Shalaby, and Z. Kawasaki, "Proposal of a hybrid OFDM-PPM technique for free space optical communications systems," in *2013 IEEE Photonics Conference*, 2013, pp. 287–288.

[56] D. Anguita, D. Brizzolara, G. Parodi, and Q. Hu, "Optical wireless underwater communication for AUV: Preliminary simulation and experimental results," in *OCEANS 2011 IEEE - Spain*, 2011, pp. 1–5.

[57] S. Arnon, "Underwater optical wireless communication network," *Optical Engineering*, vol. 49, pp. 1 –6, 2010.

[58] S. Tang, Y. Dong, and X. Zhang, "Impulse response modeling for underwater wireless optical communication links," *IEEE Transactions on Communications*, vol. 62, no. 1, pp. 226–234, 2014.

[59] A. Aminjavaheri, A. Farhang, N. Marchetti, L. Doyle, and B. F. Boroujeny, "Frequency spreading equalization in multicarrier massive MIMO," in *2015 IEEE International Conference on Communication Workshop (ICCW)*, 2015, pp. 1292–1297.

[60] G. Durisi, U. Schuster, H. Bolcskei, and S. Shamai, "Noncoherent capacity of underspread fading channels," *IEEE Transactions on Information Theory*, vol. 56, no. 1, pp. 367–395, 2010.

[61] *RESON TC 4013 - hydrophone - Hydrophones - RESON - RESON*.

[62] E. R. Brand a National Instruments, *USRP X310 High Performance Software Defined Radio*.

[63] *NEW - RESON EC6081 mk2 - preamplifier - Hydrophone Accessories - RESON*.

[64] *Guided USRP Radio Support Package Hardware Setup - MATLAB & Simulink*.

[65] *USRP Support from Communications Toolbox - Hardware Support - MATLAB & Simulink*.